NMR structural studies of protein-small molecule interactions

Shah, D.M.

Chapter 3

Inhibition of Small GTPases by Stabilization of the GDP Complex, a Novel Approach applied to Rit1, a Target for Rheumatoid Arthritis

Dipen M. Shah[1], Masakazu Kobayashi[2], Peter H. J. Keizers[1], Adriaan W.Tuin[1], Eiso AB[5], Linda Manning[3], Anna A. Rzepiela[4], Martin Andrews[2], Flip J. Hoedemaeker[3] and Gregg Siegal[1,5]*

[1] Leiden Institute of Chemistry, Leiden University, Leiden, the Netherlands.
[2] Galapagos NV, Mechelen, Belgium
[3] KeyDP, Amsterdam, the Netherlands
[4] Pyxis Discovery, Delft, the Netherlands
[5] ZoBio, Leiden, the Netherlands

Manuscript to be submitted to the Journal of Medicinal Chemistry

Abstract

A fragment based drug discovery approach has been used to discover phthalimide-based inhibitors of a novel Rheumatoid Arthritis (RA) protein target Rit1, a member of the Ras superfamily of small GTPases. NMR screening and a nucleotide exchange biochemical assay were used to discover and validate fragment hits with IC_{50}'s in the millimolar range (**1,2**) that specifically inhibit the interconversion between the GDP bound "inactive form" and the GTP bound "active form" of Rit1. Elaboration of fragment hits yielded compounds with IC_{50}'s of ~180 μM (**16e**, **17e** and **18c**) in the biochemical assay. A crystal structure of the binary Rit1:GDP complex was solved to 2.3 Å resolution, however, it proved impossible to obtain crystals with any of the Rit1 inhibitors. Instead alternative, NMR-based methods in combination with molecular docking were employed to obtain 3D structural information on the ternary complex of Rit1·GDP and inhibitor **18c**. The docking solutions show that **18c** exchanges between two binding sites that lie very close to the GDP binding pocket of Rit1. The docked structures further reveal a novel mechanism of action, where in one of the binding modes, **18c** causes a steric occlusion of the GDP and likely inhibits its dissociation.

INTRODUCTION

Rheumatoid Arthritis (RA) is a chronic degenerative disease, characterized by inflammation and erosion of the joint structures. When not treated, it leads to substantial disability and pain in the joints. The onset of RA is characterized by the inflammation of the synovial membrane ('Synovitis") which correlates with increased expression of a specific matrix-metalloproteinase (MMP) MMP1, by synovial fibroblasts (SFs). Numerous treatments for aspects of the disease are available e.g. *NSAIDS* (Non-Steroidal Anti-inflammatory Drugs) to limit inflammation and *DMARDS* (Disease Modifying Anti-Rheumatic Drugs), but most of them are found to have limited efficacy for the treatment RA in the longer term.[1] In an effort to find new targets with therapeutic value for RA, an siRNA screening strategy was undertaken. The screen uncovered a group of potential protein targets, of which a specific protein, Rit1, was involved in an early stage of the onset of RA (US patent 7,919,259 B2). Rit1 is an interesting therapeutic target as it regulates the expression and secretion of MMP1 leading to the onset of collagen degradation. Rit1 activity is upregulated in synovial fibroblasts.[2] This observation suggests that inhibition of Rit1 activity could have therapeutic benefits for RA patients.

Rit1 (Ras-like protein in all tissues) is a member of the Ras superfamily of GTPases.[3] Proteins of the Ras family, which comprises more than 150 members in humans, are small (~25 kDa) and monomeric. Ras members function as molecular switches that govern a wide variety of signal transduction pathways that regulate e.g. cellular growth, proliferation, differentiation and apoptosis.[4,5,6] GTPases carry out their cellular function by cycling between an inactive GDP bound form and an active, GTP bound form.[7] Shuttling between active and inactive forms is facilitated by two classes of regulatory proteins, namely Guanine nucleotide exchange factors (GEFs)

and GTPase activating proteins (GAPs). GEFs function by catalyzing the exchange of GDP for GTP thereby activating the G protein. In the active form, G proteins interact with downstream effectors and thus propagate further signaling events such as transcription regulation that lead to the desired biological response. The low intrinsic GTPase activity of G proteins is enhanced by interaction with GTPase activating proteins (GAPs), that down regulate signaling activity by speeding conversion to the inactive form.[8] Numerous studies have shown that proteins from the Ras family are overexpressed in about one third of human cancers and thus are implicated as oncology drug targets.[5]

Ras GTPases undergo extensive post-translational modifications that regulate their interaction with other proteins, protect them from proteolytic degradation, facilitate association with the cell membrane or determine their subcellular localization and function. Previous attempts to target this family pharmacologically have focused mainly on inhibition of post-translational modifications such as *farnesylation* or *geranylgeranylation.*[9,10,11] These inhibitors prevent membrane association of the GTPase and hence cause the loss of cellular function. However, the performance of such compounds in clinical trials has not been as good as hoped, mainly due to adverse effects and toxicity related issues.[12] Many other therapeutic approaches such as targeting prenylation and post-prenylation modifications, targeting GEFs and GAPs and the functional regulation of GDP/GTP exchange are exciting alternatives and are reviewed elsewhere .[12]

In contrast to other Ras GTPases, Rit1 lacks a known recognition signal for C terminal lipidation, which is necessary for membrane association.[13] It has been reported by a number of groups that Rit1 signals to a variety of Ras responsive transcription factors, weakly transforms NIH 3T3 cells and binds to and activates

RGL3, a novel RalGEF.[14] However, these studies also show that Rit1 fails to activate the mitogen-activated protein (MAP) kinase or phosphatidylinositol 3-kinase (PI3K)/Akt kinase signaling cascades in NIH3T3 cells, suggesting that Rit1 uses novel effector pathways to regulate proliferation, transformation and differentiation.[15,16] These alternative approaches to inhibition of Rit1 are therefore not directly available.

With a view towards finding small molecule inhibitors of Rit1, we have employed a fragment based drug discovery approach.[17] Given the large number of GTPases present in the cell and the apparent lack of post-translational modification, we sought compounds that would specifically bind to and stabilize the Rit1-GDP complex, thereby inhibiting Rit1 dependent transcription. Validated screening hits were elaborated by analogue searching and synthetic chemistry which generated phthalimide based inhibitors exhibiting a modest micromolar affinity as judged by a biochemical nucleotide exchange assay.[14] Although we were able to elucidate a 2.3 Å resolution X-ray crystal structure of Rit1 bound to GDP, attempts to soak the inhibitors into the Rit1-GDP crystals were fruitless. Therefore, we have used NMR based methods to obtain structural information to guide further compound elaboration efforts. The resulting docking model suggests that the compound binds adjacent to the GDP. The structural information is consistent with the mode of inhibition observed in the biochemical assay.

Results & Discussion

Crystal Structure of Rit1 bound to GDP

The crystal structure of Rit1 bound to GDP (Figure 1) to 2.3 Å resolution by molecular replacement using the ras-like protein TC21 as a search model (PDB: 2ERY). The crystals contained an exceptionally low solvent content (~20%) and the

protein exhibited multiple crystal contacts apparently contributing to a rather rigid overall structure as judged by the low B-factors. Not unexpectedly, the structure of Rit1 is similar to other small GTPases and consists of the canonical fold comprising a β sheet with one anti-parallel and four parallel strands surrounded by four α-helices.[18,19] Electron density was not found for the switch II loop formed by residues 79-87, likely due to flexibility. Based on structural similarity to other GTPases, the P-lobe (orange), which forms the characteristic phosphate binding loop, consists of residues Leu 27 – Lys 34 in Rit1, while the switch I loop extends from Phe 46 to Ala 57. The orientation of the GDP nucleotide is conserved and the magnesium ion is coordinated by the oxygens of the β phosphate of the nucleotide. The electron density for the GDP and magnesium ion was clearly interpretable. Further commentary on the structure is provided in the Supplementary Information (Table S1).

Screening for Rit1-GDP Specific Ligands

A strategy was employed to search for ligands specific for GDP bound Rit1, in which. Ligand screening was accomplished using TINS (Target Immobilized NMR Screening) on both the apo and GDP bound forms of the protein, screening against a fragment collection and hits that were unique for the complex were further investigated.[20,21] The PH domain of human Akt1 was used as a reference protein. Both Rit1 and the Akt1 PH domain were immobilized using Schiff's base chemistry, which at the pH used primarily targets the amino terminus. The functionality of immobilized Rit1 was determined using a nucleotide exchange assay (Supplementary Figure S1).[14] Immobilized GDP-free Rit1 was generated by incubation with alkaline phosphatase (AP) in the presence of a non-hydrolysable analogue of GTP, followed by incubation with phosphodiesterase (PDE).[22] Since

nucleotide free Rit1 rapidly precipitates, ligand screening could only be accomplished using an approach such as TINS where the protein is immobilized on a solid support.[22]

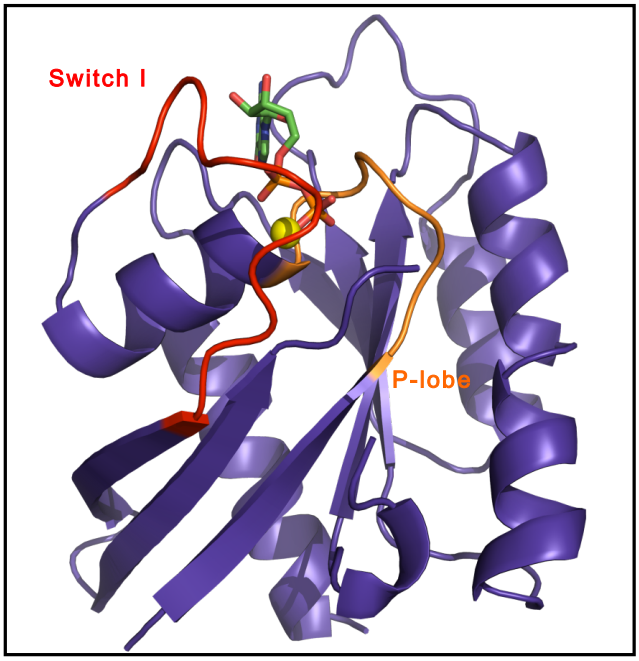

Figure 1. The crystal structure of Rit1. The switch I loop is shown in red and the phosphate recognition region, also called the P-lobe, in orange. These loops are defined based on the structural similarity of Rit1 to other GTPases.[18,19] The yellow sphere indicates the magnesium ion coordinated by the oxygens of the β phosphate of the nucleotide. The electron density for residues that form the switch II loop is missing and hence not represented in the crystal structure. The GDP is shown in sticks (green, orange, red and blue).

A library of nearly 1,000 commercially available fragments was screened against both the GDP-bound and apo-form of Rit1. The design philosophy and characteristics of the library have been previously described.[23] The hit rate observed was 3.4% and 8.8% for GDP bound- and Apo-forms of Rit1 respectively, consistent with the idea that the primary ligand binding site is the nucleotide binding pocket. The screens

resulted in the identification of 33 and 99 fragments with affinity for the GDP-bound and apo-forms of Rit1, respectively. 18 of the fragments bound both forms of Rit1, while the remaining hits bind specifically to either apo or GDP-bound Rit1.

Characterization of primary fragment hits

All hits from the TINS screen were assayed for inhibition of nucleotide exchange using purified protein.[14] Rit1 has an intrinsically slow off-rate for GDP and, since no GEF specific for Rit1 is known, it is not practical to perform the assay under equilibrium conditions.[24] Each hit from the screen was assayed at 4 mM and subsequently the IC_{50} of hits that exhibited a percentage of inhibition (PIN) above 60% was determined where possible. Since it did not prove possible to determine the IC_{50} of all weakly binding fragment hits, the fragments were ranked according to the PIN (See supplementary Figure S2). The five fragments, which exhibited a PIN greater than 60% (Figure 2) were selected for further characterization.

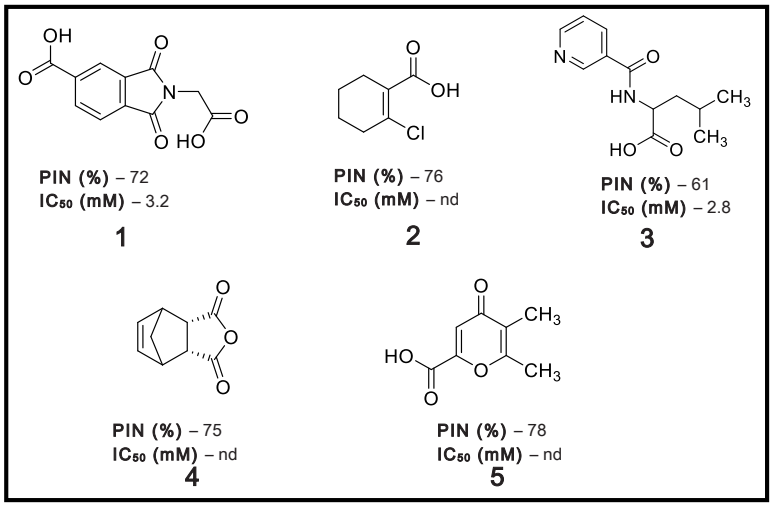

Figure 2. The five most potent fragment hits in the nucleotide exchange assay. The percentage of inhibition of the nucleotide exchange (PIN) and IC_{50} values are indicated. For fragment hits where the hill slope was too steep (>2.0), IC_{50} value could not be determined (nd).

Our repeated attempts to either soak **1** into existing crystals of Rit1·GDP or co-crystallize the ternary complex were unsuccessful. In previous reports a series of hydroxylamine bearing inhibitors were shown to inhibit the intrinsic nucleotide exchange of Ras.[25,26] The NMR based structure of a Ras-inhibitor (SCH-54292) complex revealed that the conformation of the rather flexible switch II region may be locked by the binding of the inhibitor to this region. The switch II region is known to play a role in the rate of nucleotide exchange.[25] The naphthyl moiety of SCH-54292 is buried in a hydrophobic pocket in the vicinity of switch II, while the hydroxylamine at the other end of SCH-54292 likely chelates the Mg^{2+} ion. As seen in the crystal structure of Rit1, the presence of the Mg^{2+} ion is critical for nucleotide binding and is co-ordinated by the oxygens of the β phosphate of the GDP. Based on the Ras-inhibitor (SCH-54292) NMR structure, it was hypothesized that **1** might bind to Rit1 in a pocket adjacent to GDP and in the vicinity of the Mg^{2+} atom. The carboxylic acid moiety together with one of the carbonyl groups of the phthalimide ring, was hypothesized to chelate the metal. However, with the inability to obtain a crystal structure, no conclusive experimental data was available to identify the binding site of **1**. In order to test the binding hypothesis, we sought commercially available analogues of **1**. Substructure searches were used to first find analogues containing additional molecular features on the phenyl ring of **1**. A second set of analogues was selected to replace the acetate motif on the N of the phthalimide with groups that would either ligate the Mg^{2+} tighter or provide a conformation more optimal for ligation. If metal ligation was indeed important for binding, some of these analogues would be expected to show improvement in potency in the nucleotide exchange assay. Each of the analogues was assayed for inhibition of nucleotide exchange and ranked based on the IC_{50} (Table 1).[14] Compound **6** was moderately more potent

than **1**, (~1.5 fold) while compound **7** resulted in a 4 fold increase in the potency. However, introduction of a phenyl group at R1 as in compounds **8** and **9,** results in a roughly six fold improvement in potency compared to **1**. The SAR data suggested that the carboxylic acid functionality was required at only one end of the molecule and that addition of a hydrophobic, preferably aromatic, moiety at the other end could lead to enhanced potency, although the ligand efficiency remained rather low (~0.14 pIC_{50}/Heavy atom count).[27] Interestingly, it did not appear to matter which end of the molecule contained the carboxylic acid or the aromatic ring. However, the data did not give a clear picture of whether or not metal ligation was important for binding.

Table 1. Representation of the expansion process from primary fragment hit. The table shows the features that were explored by modification of R_1 and R_2 groups resulting in the four most potent commercial analogues of **1**.

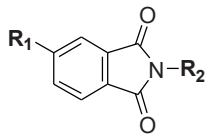

No.	R_1	R_2	Hill Slope	IC_{50} (mM)
6		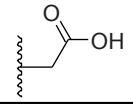	1.13	2
7	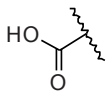	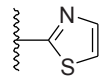	1.15	0.97
8	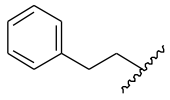	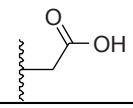	1.58	0.520
9	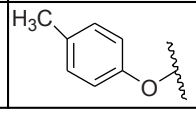	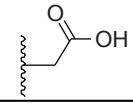	1.12	0.600

Since crystallography failed to yield structures of Rit1 with any ligand other than GDP, we turned to protein observed NMR to obtain structural information. It is well known that the 2D [^{1}H,^{15}N]-HSQC NMR experiment can provide low resolution structural information on ligand binding if the backbone resonance assignment of the protein is available. Using standard through-bond, triple resonance NMR experiments, the sequential assignment for about 72% of the backbone of Rit1 was determined (see Experimental Section). Subsequently, compound **8** was titrated into uniformly ^{15}N labeled Rit1 and residues with significant chemical shift perturbations (CSP) of the amide cross peak were identified (δH > 0.01 ppm). Potential binding sites were mapped onto the Rit1 crystal structure using the program *j-surf*.[28] Note that the NMR titration experiments were carried out at pH 9.1 as the stability of the protein was significantly greater than at pH 7.5, the pH at which the TINS screen was performed. Significant CSPs were clearly observed close to the the GDP binding site and on the opposite side of the protein close to the diphosphate moiety (Figure 3). Although this data gave us confidence that the ligand bound close to the nucleotide, it was not sufficient to precisely define the site.

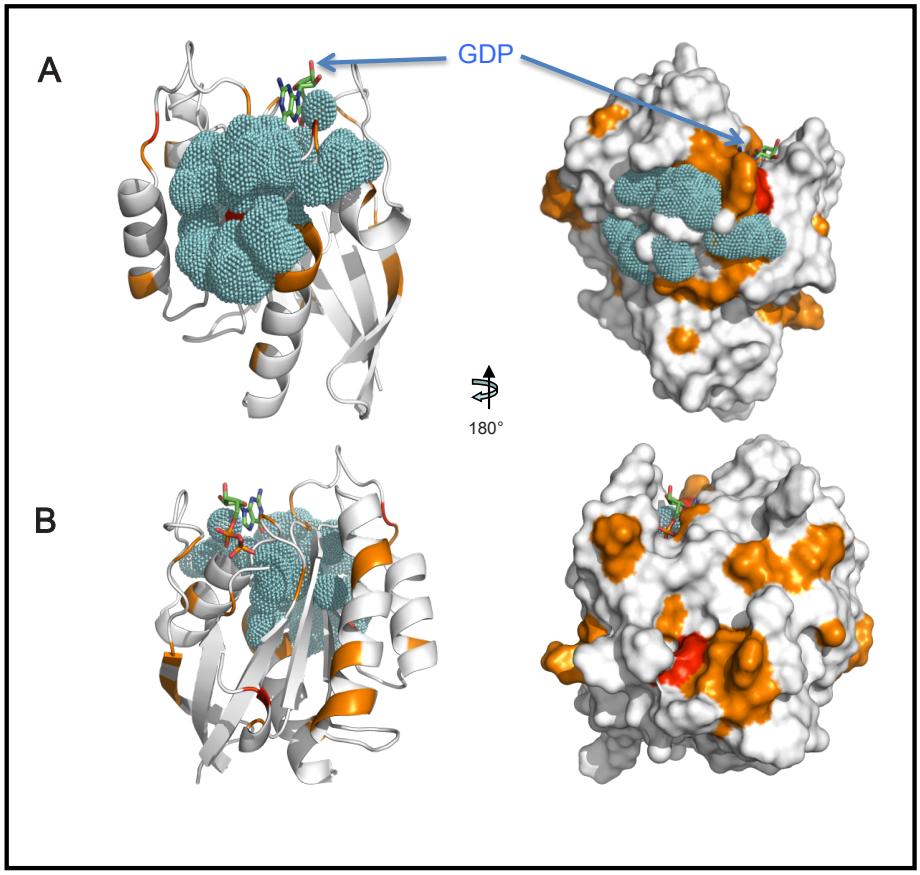

Figure 3. Mapping of the chemical shift perturbations induced by binding of **8** onto Rit1. The program j-surf was used to calculate potential binding sites.[28] The small dots forming spheres indicate the likely binding site of the compound as determined by j-surf. The red and orange colors represent the location and magnitude (larger and smaller respectively) of significant chemical shift perturbations observed on the protein. A and B show the two possible binding sites as obtained from the CSP data. This and subsequent structure figures were created in PyMOL.[29]

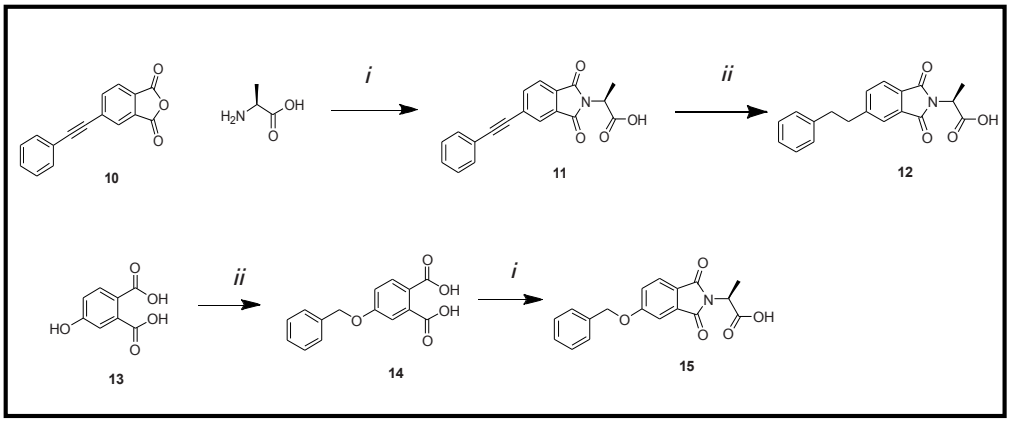

Scheme 1. Synthetic approach to elaborate compounds based **8.** Three different series of compounds **16a-e**, **17a-e** and **18a-c** (see Table 1) were accessible via this scheme. See experimental section for more information. *Reagents and conditions; i*) AcOH, MW 165°C, 5h. *ii*) EtOH, Pd/C, 2h. *iii*) BnCl, KOH, H_2O, reflux, 16h.

Elaboration of Compound 8

The chemical shift binding data, while not precisely defining the mode of interaction of **8** with Rit1, did suggest the presence of a shallow, hydrophobic patch adjacent to one of the binding sites. Based on this model, we explored the SAR around **8** using the approach outlined in scheme 1. For optimization of compound **8**, we focused on modifications of the phenyl (R_1-) and acidic (R_2-) ends of the molecule, keeping the carbon functionalized phthalimide ring structure intact. Replacement of the phenylethyl group with either a benzyl-oxy or a phenyl-ethynyl moiety resulted in compounds (**16a-d and 17a-d**) with no significant gain in potency (Table 2). The linker to the carboxylic group was modified to include a second methylene carbon to give compounds **16b** and **17b** with 2-methyl – acetic acid functionalized carbon phthalimides, however extension of the linker did not result in improved potency. The linker was then modified to include a branched methyl group with either (*S*) or (*R*) stereochemistry (**16c-d,17c-d and 18a-b**). All analogs containing the *S* stereoisomer led to reduced or unchanged potency. However, the *R* enantiomer led to significant improvement in potency with respect to the *S*

enantiomer, except in the case where the phenyl ring is connected *via* an ethyne spacer to the phthalimide core. In this latter case the reduced flexibility may affect the interaction of the acidic end of the molecule with the protein. A further significant improvement in potency (about 4 fold) was achieved by addition of a phenyl ring to the branched (*R*) methyl group resulting in compounds **16e**, **17e** and **18c**. As **18c** was found to be the most soluble of this series, it was pursued for biophysical characterization.[30,31,32]

Determining the binding site of compound 18c

Compound **18c** was titrated into ^{15}N labeled Rit1 and the chemical shift perturbations in the [^{1}H,^{15}N] HSQC experiment were again mapped onto the crystal structure (PDB 4KLZ).[33,34] The key protein residues involved in binding are Tyr 167, Tyr 169, Tyr 170 and Asp 137, which are adjacent to the GDP binding pocket. In addition to these residues, CSPs were also observed for residues 107, 110, 116, 113, 90 and 94, similar to what was observed for compound **8,** indicative of a secondary binding site. However, it is to be noted that this secondary site is close to the switch II loop of Rit1 that is missing from the crystal structure. This might suggest that these CSPs could be either due to a conformational rearrangement caused upon binding of **18c** or influenced by the flexibility of this part of the protein. As the data suggests the possibility of two binding sites, further structure restraints were necessary in order to more precisely define the nature of the binding of **18c** to the protein and to shed light on the mechanism of inhibition of nucleotide exchange. Since sidechain resonance assignments were not readily available due to the marginal quality of the NMR spectra, we chose to investigate the use of paramagnetic NMR effects for structure elucidation by introducing an organic radical (MTSL) at the 2' position of the GDP(referred to as GDP-SL).

Table 2. Analogue compounds synthesized in house by SAR on compound **8**.

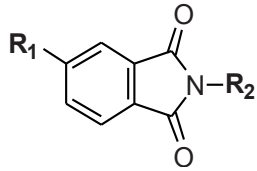

No.	R_1	R_2	Hill slope	IC_{50} (mM)
16a	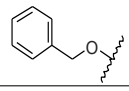		13.2	0.829
16b	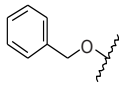		2.1	0.575
16c	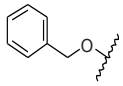		2.38	0.398
16d	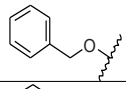		1.87	1.525
16e	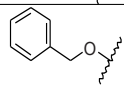		3.6	0.136

No.	R_1	R_2	Hill Slope	IC_{50} (mM)
17a	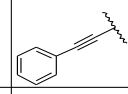	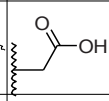	1.9	0.717
17b	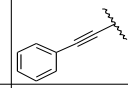	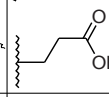	2.6	0.922
17c	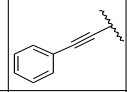		2.9	0.819
17d	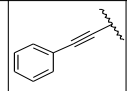		3.3	0.672
17e	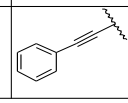		1.0	0.173

No.	R_1	R_2	Hill Slope	IC_{50}
18a	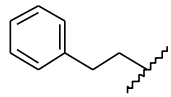	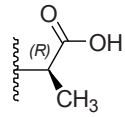	1.3	0.632
18b	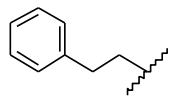	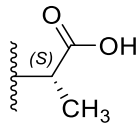	1.0	3557
18c	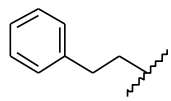	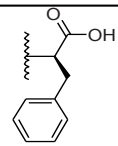	1.6	0.177

The presence of the unpaired electron of MTSL results in Paramagnetic Relaxation Enhancement (PRE) of affected NMR resonances. The PRE effect is dependent (r^{-6}) on the distance between the nucleus and the unpaired electron and can be readily calibrated by observing the effect on resonances of the protein. Determination of the PRE effects thus provides unique, long range distance information, typically from 12 to 22 Å.[35] In order to calibrate the PRE effects, a 2D [^{1}H,^{15}N] HSQC spectrum was recorded of ^{15}N labeled Rit1 with either the paramagnetic GDP-SL or diamagnetic GDP bound. For each observed amide proton, the intensity ratio (I_{para}/I_{dia}) of the resonances in the paramagnetic and diamagnetic spectra was determined, from which the PRE was converted into a distance as described.[35] The observed distances were then used to back calculate the position of the radical using the Rit1-GDP crystal structure. The average position of the nitroxide radical of the GDP-SL relative to the protein backbone could be determined with high reliability and was found to be close to the bound GDP in the crystal structure. The back-calculated nitroxide to amide proton distances match the experimentally determined distances very well, as judged by the low Q-value of 0.059 (Supplementary Figure S3). Q value is a statistical parameter in which the distances from the docking model are compared to the experimentally obtained. The smaller the value, the better the fit of back calculated versus experimental data. A model of the nitroxide spin labeled GDP bound to Rit1 was generated based on the experimental distances using XPLOR-NIH (For more details refer to the experimental section).[36] The model was subsequently used to characterize the binding of **18c**.

The PRE effect on the ^{1}H resonances of **18c** was determined by comparing the intensity of peaks in the presence of either GDP or GDP-SL bound Rit1. As seen in

Figure 4, resonances of **18c** are broadened in the presence of diamagnetic Rit1·GDP, confirming that it binds to the binary complex. Most, but not all, of the ^{1}H resonances of **18c** are further broadened beyond detection in the presence of paramagnetic Rit1·GDP-SL, indicating that they are strongly affected by the presence of the spin label. The observed PRE's were converted into distances as was done for the protein, taking into account the fractional occupancy. These intermolecular distance restraints were then used to calculate a model of the ternary complex of Rit1·GDP-SL·**18c** by docking.

Molecular Docking using PRE distance restraints

All observable protons of **18c** experience a paramagnetic effect of varying degrees due to the nitroxide radical of the GDP-SL, indicating that all protons from the compound must approach the GDP-SL for at least some part of the time (Figure 4). The docking calculations were performed using the PRE restraints, CSPs and saturation transfer effects. Saturation transfer measurements (STD) were performed to obtain structural information on the spatial proximity of ligand protons to the protein surface. This approach, also known as group epitope mapping, was originally proposed by Mayer and Meyer, 2001.[37,38,39] In the case of **18c**, the saturation transfer curves show similar kinetics for all protons suggesting that either the ligand binds in different orientations or is approximately equally surrounded by the protein on all sides. As a result, the STD data was included as ambiguous restraints in the docking procedure (Figure S6). The resulting structures exhibited a poor correlation between experimental restraints and back calculated distances with a Q-value of 0.07 (Figure S7). Specifically, the average distances in the ensemble of docked structures is consistently less than the corresponding experimental restraint with large violations.[35]

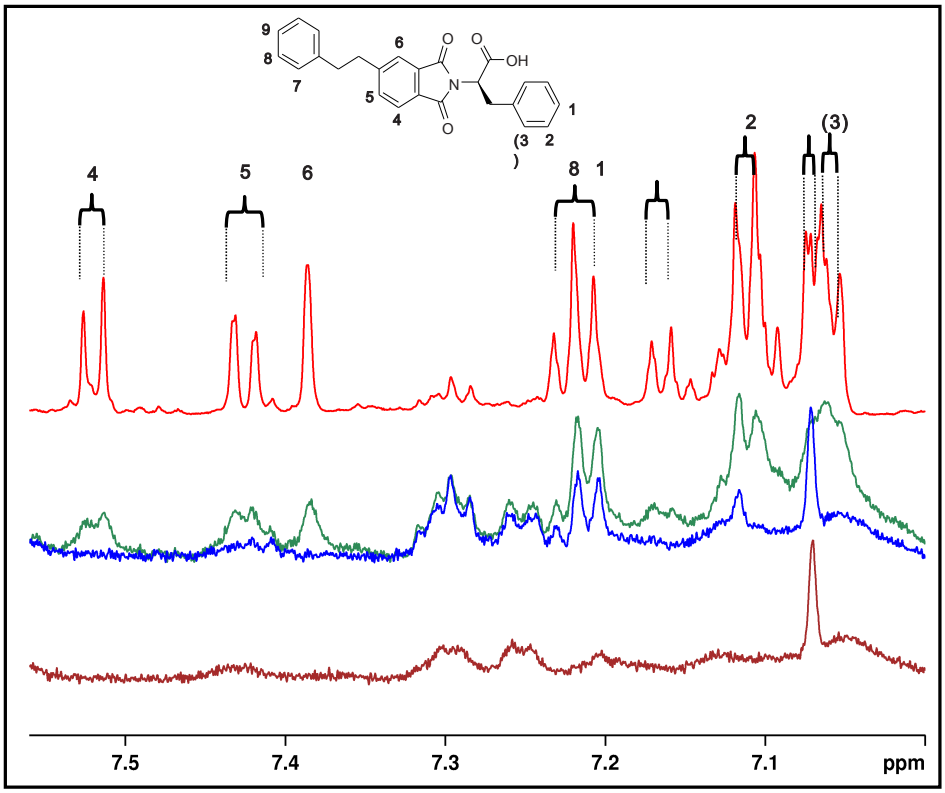

Figure 4. Paramagnetic relaxation enhancement (PRE) effect on the ^{1}H resonances of **18c** bound to Rit1·GDP-SL. The structure of compound **18c** is indicated with proton assignments. The corresponding resonances in the aromatic portion of the ^{1}H NMR spectrum are indicated. A reference spectrum of **18c** is provided (red). Peak broadening in the presence of Rit1·GDP (green) is indicative of binding. Further broadening due to PREs is clearly observed for many resonances in the presence of Rit1·GDP-SL (blue). A reference spectrum of Rit1 ·GDP-SL in the absence of **18c** is provided (brown). Due to considerable overlap in the resonances caused by the overall symmetry of **18c**, one proton (3) could not be definitively assigned and resonances arising from protons 8 and 1 could not be distinguished. The resonances from the aliphatic region of the 1D spectrum are shown in the SI (Figure S5).

The pattern of violations observed in the docking based on a single set of restraints suggests the possibility of averaging over multiple orientations or possibly binding sites. Given the symmetry of the compound, with the two phenyl groups attached to the phthalimide moiety, it is conceivable that the compound binds in two orientations. Therefore, it was decided that the PRE-based distance restraints should

be divided into two groups, i) one PRE set representing the protons of the acidic side of the compound and ii) a second PRE set representing the protons of the non-acidic side of the compound. Subsequent docking calculations were performed with either of the two sets of PRE restraints, CSPs and the ambiguous restraints from STD. The five lowest energy solutions from each of the two calculations show two minima (Figure 5). In one binding mode, defined by the restraints from the non-acidic end, **18c** lies in a shallow groove parallel to the sugar and phosphates of GDP and crosses over to occlude the base. In the second binding mode, the compound binds in the groove above the β3-strand formed by residues 160:163. Within the five lowest energy structures for each of the binding modes, **18c** is found in two orientations, rotated by approximately 180 degrees. In contrast to the calculations in which all of the PRE restraints were simultaneously used, the intermolecular distance restraints for the two ensembles of five structures fit very well to the experimentally determined distances, with a Q-value of 0.04 (supplementary Figure S7).

Discussion and Conclusion

In this work we aimed to develop small molecule inhibitors of the small GTPase Rit1, a novel target for rheumatoid arthritis.[2] We report here for the first time the crystal structure of Rit1 bound to GDP solved to 2.3 Å. This was a useful starting point, but since it proved impossible to obtain structures with the inhibitors bound did not directly aid in driving design. Thus, the elaboration of the initial 3 mM fragment hit was based on structural information obtained by NMR methods. The NMR methods were selected for the ability to rapidly generate reliable constraints for molecular docking studies and included chemical shift perturbations derived from 2D [^{1}H,^{15}N] HSQC spectra, epitope mapping by saturation transfer difference spectroscopy and paramagnetic relaxation enhancement derived intermolecular distances. The latter

two types of restraints can also be employed in cases where isotope labeling of the target is not possible. This demonstrates that NMR can provide structural information with sufficient detail and timeliness to support medicinal chemistry efforts when X-ray crystallography is not available. Although the directly modulation of GTPase activity with small molecules has proven challenging, we have been moderately successful in elaborating the phthalimide based inhibitors to an IC_{50} of approximately 180 µM. Importantly, the inhibitors have a novel mode of action.

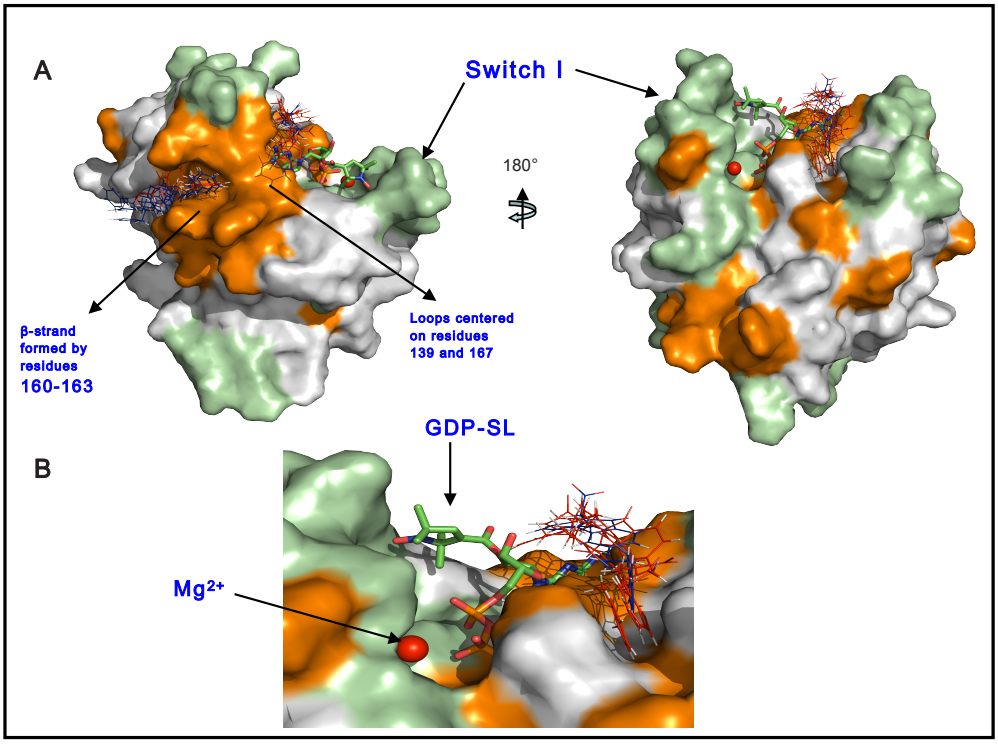

Figure 5. Experimentally restrained docking of **18c** onto the Rit1·GDP-SL complex. **A]** The lowest energy binding solutions as determined by docking using restraints from PRE, CSP and saturation transfer. The surface of Rit1 is presented and the bound GDP-SL (green) is shown in bond representation. The presence of magnesium ion is indicated by a red sphere. Compound **18c** is also shown in bond representation (narrow lines) where the two different orientations, rotated by 180°, are shown in red and blue. Amino acids with significant chemical shift perturbations observed in the presence of compound are shown in orange. The protein residues for which there are no assignments available are shown in pale green. **B]** Closeup view of one of the binding modes of compound **18c** binding adjacent to the GDP-SL (green). This binding site likely stabilizes the Rit1·GDP complex by steric hindrance of nucleotide exchange.

The Rit1·GDP·18c complex

The PRE based data and the subsequent docking results reveal that compound **18c** does not bind Rit1 in one preferred orientation or even within a single binding site. Rather, **18c** explores a large surface near the GDP binding pocket of Rit1. The two specific binding modes found in the restrained docking indicate that **18c** binds in a shallow groove. These two binding grooves are physically separated in the Rit1 crystal structure by the bulk of the loops consisting of residues 135 - 145 and 165 – 170, although at the closest points the two sites are within 6.5 Å and translocation from one site to the other could be accomplished by a simple flip (Figure 5). Interestingly, the Hill slope of 1.6, which suggests somewhat greater than 1:1 stoichiometry, is consistent with the two binding modes from the docking. In Figure 4, it is clear that protons from both phenyl rings of **18c,** which are some 12 Å distant, experience a considerable paramagnetic effect. This data means that both phenyl rings of **18c** must closely approach the MTSL during the complex formation, at least for some part of the time. For the base occluded binding mode, both ends of 18c are sufficiently close to MTSL that in principle a single orientation could explain the data, however, two orientations are found in the docking ensemble. For the binding mode close to the β3-strand, 18c must bind in both orientations (i.e. flipped 180 degrees) in order to satisfy the data. As the complex is in rapid exchange on the NMR timescale, it seems likely that the two orientations are exchanging rapidly as well and indeed, there may be additional rapid exchange between the two binding modes. To our knowledge, this is the first documented case of a small molecule exchanging between multiple binding poses, although this behavior is frequently invoked in fragment based drug discovery as a possible explanation for the failure to observe ligands in crystal structures of the target.

Neither of the binding sites of the phthalimide compounds comprises a deep

groove and in particular, the base occluded binding mode is unusual. In principal the addition of the organic radical at the 2' carbon of the sugar of GDP could perturb the structure of Rit1 and create an artificial binding site. For the β3-strand binding site, this seems particularly unlikely since the site is remote from the sugar and there is no evidence from the PRE data that the crystal structure is perturbed in this region. On the other hand, the base occluded site is adjacent to the GDP and could possibly be influenced by the presence of the MTSL. However, three observations argue against this possibility. First, the MTSL is on the other side of the GDP and does indeed perturb the structure of Rit1, but in a flexible loop distal to the proposed binding site of **18c** (Figure S4). Second, there are extensive CSPs induced by the binding of **18c** to the native Rit1:GDP complex in the base occluded binding site. This suggests that **18c** binds at this site even when the MTSL is absent. Thirdly, a truncated-driven NOE experiment suggested that the aromatic protons of a closely related compound were within 5Å of the imino proton of the base (data not shown).[40] The base occluded binding mode is most consistent with this data, even though no restraints based on the data were included in the calculation. In the base occluded model, the Mg^{2+} ion is on the opposite side of the phosphates of GDP from **18c**, therefore, it seems unlikely that the compound binds *via* metal chelation.

Novel mode of nucleotide inhibition

Recently the crystal structure of an "inactive" form of GTP bound HRas has been elucidated.[41] In this structure the Switch I loop is significantly displaced from the nucleotide, theoretically creating a potential small molecule binding site. One could speculate that if a similar Switch I displacement occurred in the GDP bound state a similar binding site might exist. However, if it does, it is on the opposite side of the nucleotide from the occluded binding mode of **18c** and we do not have

any data to suggest that **18c** nor any of the other compounds in this study might bind at such a hypothetical site. A small molecule binding site with allosteric properties has been found on KRas.[42] Interestingly, small molecules bind this site in the presence of either GDP or GTP analogues. Apparently, binding at this site inhibits the interaction with the GEF SOS. This allosteric site however is remote from the base occluded binding site (Figure 6), suggesting that 18c acts with a novel mechanism, that is steric inhibition of GDP release. This new binding site may point towards a new approach to inhibit this pharmaceutically important yet challenging class of targets.

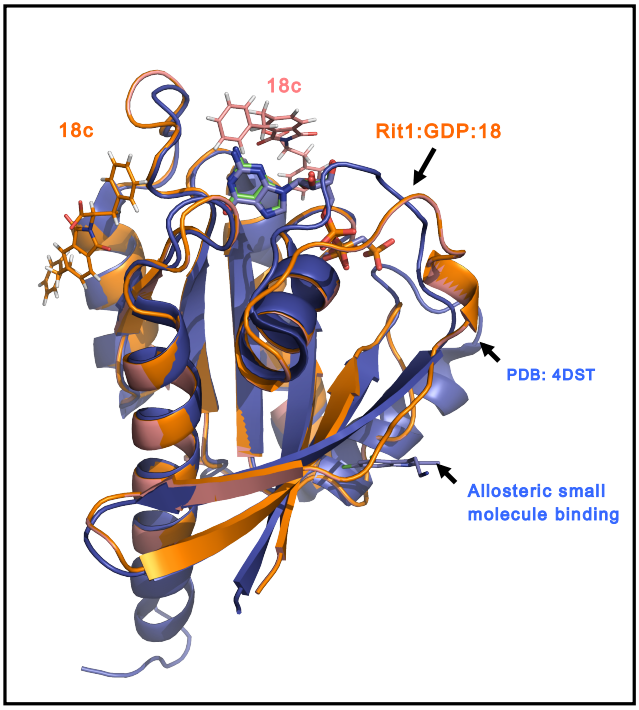

Figure 6. The comparison of the docked model of Rit1·GDP·**18c** complex with $KRas_m$·GCP:small molecule complex. The docked model of the ternary complex, Rit1·GDP-SL·**18c** (orange) is shown overlaid with and the structure of $KRas_m$·GCP:small molecule complex (blue, PDB:4DST). The two binding sites for **18c** are shown in orange and dark pink color. It is seen that **18c** binding sites are distal from the pocket 1 and switch II region but lie close to pocket 2. The allosteric binding site found for small molecule bound to $KRas_m$ lies remote from the binding sites of **18c.**[41,42]

Experimental Section
Protein Production

For X-ray crystallography, an N-terminal cleavable hexahistidine tagged-Rit1 construct (aa 19-189) was cloned into pQTEV vector and expressed in *E. coli* BL21 (DE3) codon plus (RP) (Stratagene). The protein was purified on Ni-Hitrap FF (GE lifescience) followed by purification on a superdex G75 gel filtration column (GE lifescience). The hexahistidine tag was removed by the proteolytic digestion with TEV protease (Invitrogen) according to the manufacturer recommended buffer condition. The cleaved tag and the TEV protease were removed by affinity purification on Ni-Hitrap FF, and subsequently the buffer of Rit1 (19-189) was exchanged to 20 mM Tris pH9, 5 mM NaCl, 2 mM $MgCl_2$ and 1 mM DTT.

For NMR studies, a C-terminal hexahistidine tagged-Rit1 (aa 19-189) was cloned into pET20b and expressed in *E. coli* strain BL21 (DE3) Codon Plus (RP) (Stratagene). The protein was first purified on Ni-Hitrap FF (GE lifescience) followed by purification on Superdex G75 with buffer of 20 mM Tris pH 9, 5 mM NaCl, 2 mM $MgCl_2$ and 1 mM DTT. To obtain sequential backbone resonance assignments, uniform ^{13}C, ^{15}N labeling of Rit1 was achieved by expression of C-terminally hexahistidine tagged Rit1 (aa 19-189) in BL21 (DE3) Codon Plus (RP) cells grown in M9 minimal medium supplemented with $^{15}NH_4Cl$ and ^{13}C-D-Glucose (CIL) as sole nitrogen and carbon sources. The protein was purified as described above. For protein observed HSQC studies, ^{15}N labeled C-terminal hexahistidine tagged Rit1 (aa 19-189) was produced in M9 minimal medium supplemented with $^{15}NH_4Cl$ as a sole nitrogen source and purified as described above.

For nucleotide exchange assay, a N-terminal GST (Glutathione S-transferase) tagged-Rit1 (aa 1-201) was expressed and purified as described previously.[14,43]

Crystallization and structure determination of the Rit1·GDP complex

The protein was concentrated to 10 mg/mL concentration prior to crystallization. The Rit1 crystals were grown in the presence of 11-14% w/v PEG 4000, 5-8% v/v Jeffamine M600 and immidazole buffer pH 7.0-7.2 using sitting drop vapour diffusion method. The crystals were harvested with a nylon loop and transferred to cryo-conditions by briefly passing the crystals through mother liquor augmented with approximately 30% glycerol. The crystals were then flash-frozen by exposing them to the cold-stream of the X-ray source. All the diffraction data was collected using a Cu-Kα rotating anode X-ray generator and a CCD area detector. The best diffracting crystals grew on the plastic surface of the crystallization well and diffracted up to 2.3 Å on a rotating anode X-ray beam. The diffraction data were integrated and scaled with the PROTEUM*plus* Crystallographic Software Suite by Bruker AXS and processed by CCP4 (Collaborative Computational Project, Number 4. 1994).[44] The structure of the protein was solved by Molecular Replacement, using the ras-like protein TC21 (PDB: 2ERY); 55% sequence identity) as a search model. Molecular replacement was carried out with the *MOLREP* routine in *CCP4* by searching for one molecule in the asymmetric unit. The refinement of the MR solution was carried out using *REFMAC5* from *CCP4*. Model building for the structure of Rit1 was carried out with the program *COOT.* [44,45]. The co-crystallization and soaking trial experiments for protein compound complex were unsuccessful and caused protein crystals to crack.

TINS NMR screening

Rit1 (aa 19-189) and Akt PH domain (aa 1-123) were immobilized via amine-coupling to 500 µL Actigel-ALD resin (Sterogene) in 25 mM Hepes pH 7.5, 100 mM

NaCl and 2 mM $MgCl_2$ at 4°C using the coupling reagent provided by the manufacturer. Due to low solubility of Rit1 at pH 7.5, the protein was immobilized in consecutive addition at 50 μM. The immobilization efficiency was above 90% and the final concentrations of the immobilized targets were typically in the range of 500 μM. The immobilized Rit1 was shown functional by the nucleotide exchange activity (Shao, H, et al 2000).[14,43] TINS NMR experiments were performed on 500 MHz Bruker NMR spectrometer using spatially selective Hadamard pulse sequences and analyzed as described previously.[20,46,47] GDP-bound Rit1 was immobilized as described above. The composition of the fragment library screened has been reported previously.[23] The typical fragment mix applied to the immobilized proteins consisted of 3 ~ 5 fragments which were each at 500 μM. The buffer used in the screen was comprised of 25 mM Tris-d_{11} pH 7.5, 100 mM NaCl, 1 mM $MgCl_2$ for GDP-bound from of Rit1.

In vitro nucleotide exchange assay / High concentration bioassay

The nucleotide exchange was determined by the rapid filtration technique. The exchange buffer comprised of 1 μM of GST-Rit1 (aa 1-201), 2 μM [^{32}S] GTPγS (2 Ci/mmol, PerkinElmer) in 25 mM Tris pH 7.5, 100 mM NaCl, 1 mM DTT and 0.5 mM $MgCl_2$ (on ice), and then the spontaneous nucleotide exchange was initiated by incubation at 30°C. After 1 hour incubation at 30°C, the [^{32}S] GTPγS bound GST fusion protein was isolated onto 96-well Unifilter GF/B using Filteramate harvester (PerkinElmer) with cold wash buffer of 25 mM Tris pH 7.5, 100 mM NaCl, 1 mM DTT and 10 mM $MgCl_2$. The filter was soaked in Microsint scintillation fluid and the bound [^{32}S] GTPγS was detected using TopCount (PerkinElmer). All the fragments determined as hits specific to Rit1 from TINS NMR screening were subjected to high

concentration bioassay. Initially, the total nucleotide exchange was monitored in the presence of fragment or in DMSO. The amount of DMSO in the controls was matched to 1.5% (v/v), which is equivalent to the amount in the presence of a fragment. In 96 wells, 8 wells containing either DMSO or 400 μM of GDP were employed as internal controls. The percentage of inhibition (PIN) was determined as follows: PIN (%) = [1 - ($A_{fragment} - A_{positive\ control}$) / ($A_{negative\ control} - A_{positive\ control}$)] x 100%, where $A_{fragment}$ and $A_{negative\ control}$ are the radioactive counts measured in the presence of fragments and DMSO, respectively, whereas $A_{positive\ control}$ is the radioactivity measured in the presence of 400 μM of GDP that competed out [^{35}S] GTPγS for the nucleotide site in Rit1. The diagrammatic representation of the nucleotide exchange assay is shown in Figure S10.

NMR backbone sequential assignment

The following NMR experiments were acquired at 293K on an 800 MHz Varian Inova spectrometer; [^{1}H,^{15}N] -HSQC, HNCO, HNCA, HNCACB, CBCACONH and 3D [^{1}H,^{15}N] NOESY-HSQC.[33,34] The protein sample consisted of 0.5 mM Rit1 (aa 19-189) in 25 mM d_{11}-Tris pH9, 5 mM NaCl and 5 mM $MgCl_2$. The data was processed using NMRPipe and visualized using Sparky.[48,49] The assignment process was guided by the automatic assignment program MARS using PDB 4KLZ as an input.[50]

Chemical shift perturbation and generation of binding site

The [^{1}H, ^{15}N]-HSQC were acquired at 298K on 600 MHz Bruker DMX NMR spectrometer equipped with a TXI cryo-probe.[33,34] The NMR sample was prepared in 25 mM Tris pH 9, 5 mM NaCl and 5 mM $MgCl_2$. The typical NMR sample contained 0.125 mM of the protein, compounds at various concentrations (see text) and 5% d_6-

DMSO. The pH of the samples was adjusted carefully within +/- 0.05 units after addition of the compound. During the experiment, total of 128 indirect increments with 16 scans per increments were acquired. The data was processed using Topspin 1.2/2.1 (Bruker) and visualized on Sparky.[49] Chemical shift perturbation in [^{1}H, ^{15}N]-HSQC was calculated for change in ^{1}H ppm value between in the presence and absence of a compound. The potential binding sites of a compound were mapped onto the surface of the Rit1 structure by *jsurf* using chemical shift perturbation data (delta ^{1}H ppm) as input.[28]

Saturation Transfer Experiments

Saturation transfer NMR experiments were conducted using pulse sequences as described.[37,38,39] The protein concentration was 40 μM and compound was present at a 20 fold in molar ratio. The pH of the sample was adjusted carefully within +/- 0.05 units. The on-resonance irradiation of the protein was performed at -0.5 ppm and off-resonance irradiation was performed at 100 ppm where no protein signals are present. The saturation time was varied between 50 ms to 2 sec in order to determine the buildup rate. No significant differences in the buildup rate between the protons were observed (see supplementary figure S6).

Paramagnetic NMR Studies

Synthesis of GDP-Spin label

The procedure followed was modified from literature.[51,52,53] One equivalent each of 3-Carboxy-2,2,5,5-tetramethyl-3-pyrrolin-1-yloxy, Free Radical (Toronto Research Chemicals) and N,N-carbonyldiimizdazole (dissolved in dimethyl formamide) were mixed together and incubated for 1 hour. To this one equivalent of

guanosine diphosphate sodium salt (Sigma) was added and incubated further for 1 hour at 38°C water bath while stirring and pH adjusted to 9.1 using 1 M NaOH. The reaction mixture was extracted twice with chloroform and pH of the aqueous phase was adjusted to pH 7.5 with 1N acetic acid. The solution was filtered and was further subjected to LCMS analysis using reversed-phase HPLC purification using an automated HPLC system supplied with a semi-preparative C_{18} column (10.0 mmD × 250 mmL, 5 μ particle size) was used. Mass spectra were recorded for elutes and yielded the product of expected size. Purified elutes were further lyophilized and gave a typical pale yellow color, characteristic of the presence of nitroxide radical. The presence of radical was further confirmed by acquiring an EPR spectrum. The X-band cw EPR measurements were performed using an ELEXSYS E680 spectrometer (Bruker, Rheinstetten, Germany) equipped with a rectangular cavity. A modulation frequency of 100 kHz was used. Measurements were done at temperature of 20°C, using 6.31 mW of microwave power and modulation amplitude of 0.5 G (See Figure S8 in supplementary).

PRE studies on Protein

The removal of GDP was performed by buffer exchange into 20 mM HEPES pH 7.5, 1 mM EDTA, 1 M $(NH_4)_2SO_4$, 20 % glycerol.[54] The GDP removal was checked by disappearance of a peak at 260 nm in the UV absorption spectrum. The ability of apo-Rit1 to bind to chemically modified GDP was checked by a fluorescent based- assay. In this assay, MANT-GDP [(2'-(or-3')-O-(N-methylanthraniloyl) guanosine 5'-diphosphate] (Biolog, Germany) was titrated into apo-Rit1 and change in the intensity of the MANT fluorescence caused by binding to Rit1 was measured in a concentration dependant manner. The results showed that MANT-GDP bound with

a 1:1 stoichiometry to apo-Rit1. As MANT-GDP carries a similar chemical modification at the ribose moiety of GDP as in the GDP-SL, we assumed that this would lead only to a minimal perturbation of Rit1-GDP-SL interaction (data not shown). The protein was exchanged back into the buffer composed of 25 mM Tris pH 9, 5 mM NaCl and 5 mM $MgCl_2$. The paramagnetic GDP-SL was added at a 1.5 molar excess over protein, incubated on ice for 30 min and then washed three times with 25 mM Tris pH 9, 5 mM NaCl and 5 mM $MgCl_2$ using a Centricon centrifugal concentrator with MWCO 10 kDa (Millipore). The same procedure was followed during preparation of diamagnetic control sample except that diamagnetic GDP (SIGMA) was added. The protein concentrations used were identical during NMR measurements. NMR samples contained, a paramagnetic sample consisting of 0.1 mM Rit1 bound to GDP-SL and a diamagnetic control consisting of 0.1 mM Rit1 bound to GDP in 25 mM Tris pH 9, 5 mM NaCl and 5 mM $MgCl_2$, 5%D_2O. The measurements were performed at 298 K on 600 MHz Bruker DMX NMR spectrometer equipped with a TXI cryo-probe. During the experiment, total of 128 indirect increments with 16 scans per increments were acquired. The data was processed using Topspin 2.1 (Bruker) and visualized using Sparky.[49]

PRE studies on compound 18c

C-terminally hexahistidine tagged Rit1 (aa 19-189) was expressed and purified as described above. The paramagnetic and diamagnetic protein samples were made as described above. The compound was added to the protein sample at a ratio of 1:1. 1D proton NMR spectra were acquired at 298 K on 600 MHz Bruker DMX NMR spectrometer equipped with a TXI cryo-probe. A CPMG delay of 40 ms was used to suppress residual protein signals. The data was processed using Topspin 2.1

(Bruker). For each observed amide proton, the intensity ratio (I_{para}/I_{dia}) of the resonances in the paramagnetic and diamagnetic spectra was determined, from which the PRE was converted into a distance as described.[35] The minor variations in the intensities for the compound signals in the 1D spectrum diamagnetic and paramagnetic sample of **18c** in the presence of the protein were referenced to the signal from DMSO.

Docking of Rit1·GDP·18c ternary complex

PREs of amide protons of the protein were obtained from peak intensities in HSQC spectra of paramagnetic and diamagnetic protein and subsequently used to determine the position of the nitroxide radical relative to the protein crystal structure. For this, the interatomic proton to radical distances were determined from the PREs as described,[35,55] using an experimentally determined correlation time of 11.5 ns. The correlation time was determined using [^{1}H,^{15}N] HSQC analysis with varying T1 and T2 delays The distances were divided into three different classes. The protons for which the resonances were broadened beyond detection, were given an upper limit of 14 + 3/-8 Å, protons of which the resonances were unaffected, were given a lower limit of 21 + 100/-3 Å. The distances for 27 protons, lower limits for 25 and upper limits for 5 protons were used to obtain the energy minimum of the nitroxide radical using XPLOR-NIH.[36]

The compound was docked onto the GDP-SL·Rit1 complex using XPLOR-NIH using experimental restraints from the CSPs data by HSQC NMR titration (some CSPs are shown in Figure S9), saturation transfer and paramagnetic experiments.[36] Based on the measured PREs, 10 distances between ^{1}Hs of **18c** including two aliphatic protons and the nitroxide were obtained. Large CSPs of 13 amides as

determined by titrating the compound into the protein as determined by HSQC, were translated into ambiguous distance restraints of 6 +/- 3 Å to any compound proton while averaging over $<r^{-6}>$. Similarly, based on the saturation transfer experiments, ambiguous distance restraints of 5 + 4/-3 Å were applied between any compound proton and any protein carbon atom. Protons were subsequently added manually. In a typical simulation, the compound approached the protein 10,000 times, where the compound was placed at a random position every four approaches the energy did not drop. The compound was treated flexible and was initially docked on the backbone of the protein including Cα and Cβ followed by inclusion and optimization of the sidechains. (The docking script is provided in the Supplementary Information; S12). The docking results are evaluated by a Q-value.[35] In this statistical parameter distances from the docking model are compared to the experimentally obtained. The smaller the value, the better the fit of back calculated versus experimental data.

Model Structure of GDP-Spin Label

A structure of 3-carboxy-2,2,5,5-tetramethyl-3-pyrrolin-1-yloxy was prepared in Spartan (www.wavefun.com) and parameterized using the Prodrugserver.[56] The chemical structure of the GDP spinlabel probe is shown is Figure S11. Additional dihedral and angle parameters were added to keep the nitroxide in plain with the pyrroline ring. The molecule was added to the protein and attached to the GDP using XPLOR-NIH. To this end, an ester linkage was created between the carboxylate and the 2'- hydroxyl of the GDP and the nitroxide oxygen atom was moved in the direction of the predetermined minimum energy position. The spin-labeled GDP was energy minimized, before optimizing the loop consisting of residues 42:57, surrounding the GDP based on 15 PREs determined for these residues

(Supplementary Figure S4).

Synthesis of elaborative compounds based on compound 8:

Carbon functionalized phthalimides are synthesized analogues to the literature procedure **(**Scheme 1).[i] Commercially available 4-phenylenthynylphthalic anhydride **10** is condensed with the appropriate amino acid in acetic acid under microwave irradiation at 165°C for four to five hours yielding the desired products in yields ranging from 80% to 97% after recrystallization or HPLC purification. Hydrogenation of the triple bond using palladium on charcoal afforded saturated phthalimides similar to **12** in yields ranging from 74% to 99% after HPLC purification. Oxygen functionalized phthalimides such as **15** were synthesized from 4-benzyloxyphthalic acid[ii] (**14**) in yields ranging from 43% to 78%.[30,31]

General: PE with a boiling range of 40 - 60°C was used. THF and Et_2O were distilled over $LiAlH_4$ prior to use. DCM (dichloromethane) was distilled over CaH_2 prior to use. All other solvents used under anhydrous conditions were stored over molecular sieves (4Å) except for methanol which was stored over 3Å molecular sieves. Solvents used for work-up and column chromatography were of technical grade and distilled before use. Microwave assisted reaction were carried out in an Emrys Optimizer (Biotage AB, formerly Personal Chemistry). Wattage was adjusted automatically so as to maintain the desired temperature. Unless stated otherwise, solvents were removed by rotary evaporation under reduced pressure at 40°C. Reactions were monitored by TLC-analysis using DC-fertigfolien (Schleicher & Schuell, F1500, LS254) with detection by spraying with 20% H_2SO_4 in EtOH, $(NH_4)_6Mo_7O_{24}\cdot 4H_2O$ (25 g/L) and $(NH_4)_4Ce(SO_4)_4\cdot 2H_2O$ (10 g/L) in 10% sulfuric acid or by spraying with a solution of ninhydrin (3 g/L) in EtOH / AcOH (20/1 v/v), followed

by charring at ~150°C. Column chromatography was performed on Fluka silicagel (0.04 – 0.063 mm). For LC/MS analysis, an JASCO HPLC-system (detection simultaneously at 214 and 254 nm) equipped with an analytical C_{18} column (4.6 mmD × 250 mmL, 5μ particle size) in combination with buffers A: H_2O, B: MeCN and C: 0.5% aq. TFA and coupled to a mass instrument with a custom-made Electronspray Interface (ESI) was used. For reversed-phase HPLC purification of the final compounds, an automated HPLC system supplied with a semi-preparative C_{18} column (10.0 mmD × 250 mmL, 5 μ particle size) was used. The applied buffers were A: H_2O, B: MeCN and C: 1.0% aq. TFA. High resolution mass spectra were recorded by direct injection (2 μL of a 2 μM solution in water/acetonitrile; 50/50; v/v and 0.1% formic acid) on a mass spectrometer (Thermo Finnigan LTQ Orbitrap) equipped with an electrospray ion source in positive mode (source voltage 3.5 kV, sheath gas flow 10, capillary temperature 250°C) with resolution R = 60000 at m/z 400 (mass range m/z = 150-2000) and dioctylpthalate (m/z = 391.28428) as a "lock mass".[iii] The high resolution mass spectrometer was calibrated prior to measurements with a calibration mixture (Thermo Finnigan). ^{1}H- en ^{13}C-NMR spectra were measured on a Joel JNM-FX-200 (200/50 MHz). Chemical shifts are given in ppm (δ) relative to TMS (0 ppm) or MeOD (3.30 ppm) and coupling constants are given in *Hz*.[32,57,58]

General condensation procedure: Phthalic acid or anhydride and the appropriate amino acid (1.05 equiv) are suspended in acetic acid (5 mL) and the reaction mixture is heated in a sealed tube for five hours at 165°C in the microwave. The reaction mixture is concentrated and purified by HPLC or by means of recrystalization.[57,58,59]

General hydrogenation procedure: The appropriate alkyne is dissolved in ethanol (2 ml) and treated with Pd/C (10 mg) and hydrogen gas for 2 hours at r.t. after which the catalyst is removed by filtration over a pad of celite. The filtrate is

concentrated and the residue is, if required, purified by HPLC.

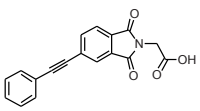

17a: Prepared from **10** (1.24 g, 5 mmol) and glycine (394 mg, 5.25 mmol) according to the general condensation procedure and purified by recrystallization from hot water. Yield: 1.48 g, 4.85 mmol, 97% off white solid. ^{1}H NMR (400 MHz, DMSO) δ 13.18 (bs, 1H, CO_2H), 8.05 (s, 1H), 8.01 (dd, *J* = 1.3, 7.7, 1H), 7.96 (d, *J* = 7.7, 1H), 7.67 – 7.60 (m, 2H), 7.50 – 7.43 (m, 3H), 4.33 (s, 2H). ^{13}C NMR (101 MHz, DMSO) δ 168.74, 166.52, 166.43, 137.34, 131.99, 131.71, 130.53, 129.60, 128.84, 128.60, 125.77, 123.78, 121.36, 93.51, 87.88, 39.02. LC-MS: *t*R: 7.91 min (linear gradient 10-90% in 13.5 min), m/z = 611.1 $[2M+H]^+$, 306.1 $[M+H]^+$, 259.9 $[M-CO_2+H]^+$

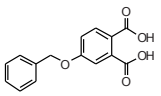

14: Prepared according to literature procedure. Yield: 5.66 g, 20.8 mmol, 76%. ^{1}H NMR (400 MHz, MeOD) δ 7.94 (d, *J* = 8.5, 1H), 7.49 – 7.26 (m, 6H), 7.13 (d, *J* = 8.6, 1H), 5.15 (s, 2H). ^{13}C NMR (101 MHz, MeOD) δ 172.33, 170.53, 162.56, 138.18, 137.83, 133.95, 129.86, 129.58, 129.12, 128.68, 124.84, 117.32, 116.89, 71.30.

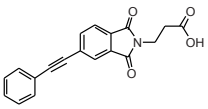

17b: Prepared from **10** (496 mg, 2 mmol) and β-alanine (187 mg, 2.1 mmol) according to the general condensation procedure and recrystallized from EtOAc/PE. Yield: 549 mg, 1.7 mmol, 85% as white solid. ^{1}H NMR (400 MHz, DMSO) δ 12.38 (bs, 1H), 7.99 – 7.94 (m, 2H), 7.89 (d, *J* = 7.6, 1H), 7.65 – 7.60 (m, 2H), 7.49 – 7.44 (m, 3H), 3.80 (t, *J* = 7.4, 2H), 2.62 (t, *J* = 7.4, 2H). ^{13}C NMR (101 MHz, DMSO) δ 172.04, 166.92, 166.83, 136.96, 132.24, 131.68, 130.86, 129.55, 128.83, 128.14, 125.37, 123.39, 121.39, 93.20, 87.95, 33.72, 32.25. LC-MS: *t*R: 7.91 min (linear gradient 10-90% in 13.5 min), m/z = 319.9 $[M+H]^+$, 302.1 $[M-H_2O+H]^+$, 259.9 $[M-CH_2CO_2+H]^+$

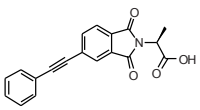

17c: Prepared from **10** (496 mg, 2 mmol) and alanine (187 mg, 2.1 mmol) according to the general condensation procedure and purified by recrystallization from hot water yielding the title compound as white solid (522 mg, 1.6 mmol, 81%).[1]H NMR (400 MHz, DMSO) δ 13.14 (s, 1H), 8.05 – 7.99 (m, 2H), 7.94 (dd, *J* = 0.6, 7.7, 1H), 7.67 – 7.61 (m, 2H), 7.50 – 7.45 (m, 3H), 4.89 (q, *J* = 7.3, 2H), 1.56 (d, *J* = 7.3, 3H). [13]C NMR (101 MHz, DMSO) δ 170.89, 166.45, 166.35, 137.31, 131.89, 131.71, 130.46, 129.60, 128.85, 128.51, 125.66, 123.69, 121.35, 93.43, 87.91, 47.11, 14.74. LC-MS: *t*R: 8.33 min (linear gradient 10-90% in 13.5 min), m/z = 320.0 $[M+H]^+$, 274.0 $[M-CO_2+H]^+$

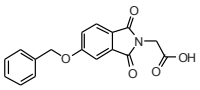

16a: Prepared from **14** (516 mg, 2 mmol) and glycine (157 mg, 2.1 mmol) according to the general condensation procedure to yield to title compound as white solid (440 mg, 1.41 mmol, 70%). [1]H NMR (400 MHz, DMSO) δ 13.13 (s, 1H), 7.85 (d, *J* = 8.3, 1H), 7.52 (d, *J* = 2.2, 1H), 7.48 (d, *J* = 7.1, 2H), 7.44 – 7.39 (m, 3H), 7.38 – 7.32 (m, 1H), 5.32 (s, 2H), 4.28 (s, 2H). [13]C NMR (101 MHz, DMSO) δ 168.92, 166.89, 166.80, 163.59, 136.02, 134.06, 128.54, 128.14, 127.82, 125.25, 123.37, 120.95, 109.26, 70.22. LC-MS: *t*R: 7.10 min (linear gradient 10-90% in 13.5 min), m/z = 312.2 $[M+H]^+$, 265.9 $[M-CO_2+H]^+$

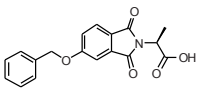

15: Prepared from **14** (516 mg, 2 mmol) and alanine (187 mg, 2.1 mmol) according to the general condensation procedure to yield to title compound as white solid (509 mg, 1.56 mmol, 78%). [1]H NMR (400 MHz, DMSO) δ 13.04 (s, 1H), 7.82 (d, *J* = 8.3, 1H), 7.51 – 7.45 (m, 3H), 7.44 – 7.38 (m, 3H), 7.38 – 7.32 (m, 1H), 5.32 (s, 2H), 4.83 (q, *J* = 7.3, 1H), 1.54 (d, *J* = 7.3, 3H). [13]C NMR (101

MHz, DMSO) δ 171.09, 166.80, 166.75, 163.56, 136.04, 133.94, 128.81, 128.54, 128.46, 128.42, 128.12, 127.78, 127.57, 125.17, 123.28, 120.96, 109.14, 70.19, 46.93, 14.87. LC-MS: *t*R: 7.56 min (linear gradient 10-90% in 13.5 min), m/z = 326.1 $[M+H]^+$, 280.0 $[M-CO_2+H]^+$

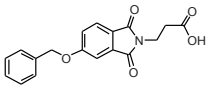

16b: Prepared from **14** (516 mg, 2 mmol) and β-alanine (187 mg, 2.1 mmol) according to the general condensation procedure to yield to title compound as white solid (500 mg, 1.54 mmol, 77%). ^{1}H NMR (400 MHz, DMSO) δ 12.35 (s, 1H), 7.77 (d, *J* = 8.3, 1H), 7.49 – 7.31 (m, 7H), 5.29 (s, 2H), 3.76 (t, *J* = 7.3, 2H), 2.59 (t, *J* = 7.3, 2H). ^{13}C NMR (101 MHz, DMSO) δ 172.09, 167.19, 163.32, 136.08, 134.20, 128.82, 128.53, 128.40, 128.11, 127.77, 127.55, 124.87, 123.59, 120.52, 108.94, 70.14, 33.58, 32.43. LC-MS: *t*R: 7.26 min (linear gradient 10-90% in 13.5 min), m/z = 326.0 $[M+H]^+$, 308.2 $[M-H_2O+H]^+$, 266.0 $[M-CH_2CO_2+H]^+$

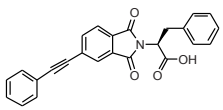

16e: Prepared from **10** (496 mg, 2 mmol) and phenylalanine (347 mg, 2.1 mmol) according to the general condensation procedure and purified by HPLC yielding the title compound as off white foam (639 mg, 1.6 mmol, 80%). ^{1}H NMR (400 MHz, DMSO) δ 13.30 (bs, 1H), 7.91 (d, *J* = 6.6, 2H), 7.83 (d, *J* = 8.0, 1H), 7.62 – 7.56 (m, 2H), 7.43 (d, *J* = 4.8, 3H), 7.19 – 7.14 (m, 4H), 7.14 – 7.07 (m, 1H), 5.16 (dd, *J* = 4.7, 11.5, 1H), 3.52 (dd, *J* = 4.7, 14.1, 1H), 3.43 – 3.31 (m, 1H). ^{13}C NMR (101 MHz, DMSO) δ 169.99, 166.43, 166.34, 137.43, 137.27, 131.70, 131.29, 129.80, 129.58, 128.81, 128.73, 128.33, 126.59, 125.77, 123.77, 121.38, 93.66, 87.77, 53.17, 33.98. LC-MS: *t*R: 9.42 min (linear gradient 10-90% in 13.5 min), m/z = 396.1 $[M+H]^+$, 350.0 $[M-CO_2+H]^+$

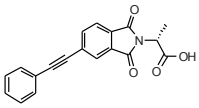

17c: Prepared from **10** (496 mg, 2 mmol) and D-alanine (187 mg, 2.1 mmol) according to the general condensation procedure and purified by recrystalization from hot water yielding the title compound as white solid (506 mg, 1.6 mmol, 80%). ^{1}H NMR (400 MHz, DMSO) δ 13.15 (s, 1H), 8.04 – 7.98 (m, 2H), 7.93 (d, *J* = 7.7, 1H), 7.66 – 7.60 (m, 2H), 7.50 – 7.45 (m, 3H), 4.89 (q, *J* = 7.2, 1H), 1.56 (d, *J* = 7.3, 3H). ^{13}C NMR (101 MHz, DMSO) δ 170.90, 166.46, 166.36, 137.30, 131.89, 131.71, 130.46, 129.59, 128.84, 128.53, 125.66, 123.69, 121.36, 93.44, 87.91, 47.13, 14.75. LC-MS: *t*R: 8.31 min (linear gradient 10-90% in 13.5 min), m/z = 320.0 $[M+H]^+$, 273.9 $[M-CO_2+H]^+$

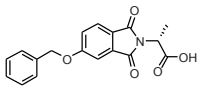

16c: Prepared **14** (496 mg, 2 mmol) and D-alanine (187 mg, 2.1 mmol) according to the general condensation procedure and purified by HPLC to yield the title compound as white solid (280,7 mg, 0.86 mmol, 43%). ^{1}H NMR (400 MHz, DMSO) δ 13.05 (bs, 1H), 7.82 (d, *J* = 8.3, 1H), 7.51 – 7.45 (m, 3H), 7.44 – 7.38 (m, 3H), 7.38 – 7.32 (m, 1H), 5.32 (s, 2H), 4.83 (q, *J* = 7.3, 1H), 1.53 (d, *J* = 7.3, 3H). ^{13}C NMR (101 MHz, DMSO) δ 171.06, 166.78, 166.73, 163.55, 136.03, 133.93, 128.53, 128.11, 127.77, 125.16, 123.26, 120.97, 109.13, 70.17, 46.90, 14.85. LC-MS: **16c** did not ionize, preventing acquisition of the LC-MS specrum

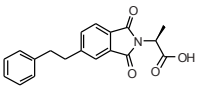

18b: Prepared from **17c** (133 mg, 0.35 mmol) according to the general hydrogenation procedure and purified by HPLC to yield the title compound (84 mg, 0.26 mmol, 74%) ^{1}H NMR (400 MHz, DMSO) δ 7.74 (d, *J* = 7.7, 2H), 7.63 (d, *J* = 8.5, 1H), 7.28 – 7.18 (m, 4H), 7.15 (t, *J* = 6.9, 1H), 4.85 (q, *J* = 7.2, 1H), 3.05 (t, *J* = 7.8, 2H), 2.91 (t, *J* = 7.8, 2H), 1.56 (d, *J* = 7.3, 3H). ^{13}C NMR

(101 MHz, DMSO) δ 171.24, 167.37, 167.23, 149.55, 140.87, 134.75, 131.84, 129.29, 128.52, 128.36, 126.09, 123.38, 123.26, 47.12, 37.19, 36.75, 14.93. LC-MS: *t*R: 7.97 min (linear gradient 10-90% in 13.5 min), m/z = 324.1 $[M+H]^+$, 278.1 $[M-CO_2+H]^+$

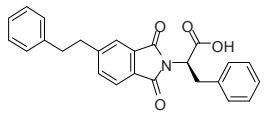

18c Prepared from **17e** (138 mg, 0.35 mmol) according to the general hydrogenation procedure to yield the title compound (141 mg, 0.35 mmol, quant). ^{1}H NMR (400 MHz, DMSO) δ 7.69 (d, *J* = 7.5, 2H), 7.60 (d, *J* = 8.2, 1H), 7.28 – 7.06 (m, 10H), 5.12 (dd, *J* = 4.8, 11.7, 1H), 3.50 (dd, *J* = 5.1, 14.9, 2H), 3.42 – 3.34 (m, 1H), 3.05 – 2.96 (m, 2H), 2.93 – 2.84 (m, 2H).^{13}C NMR (101 MHz, DMSO) δ 170.24, 167.28, 167.14, 149.66, 140.84, 137.41, 134.81, 131.21, 129.10, 128.74, 128.65, 128.44, 128.33, 128.29, 126.57, 126.02, 123.41, 123.27, 52.99, 37.08, 36.57, 34.06. LC-MS: *t*R: 9.00 min (linear gradient 10-90% in 13.5 min), m/z = 400.0 $[M+H]^+$,354.0 $[M-CO_2+H]^+$

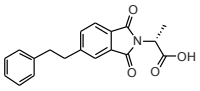

18a Prepared from **17c** (99.5 mg, 0.31 mmol) according to the general hydrogenation procedure to yield the title compound (93 mg, 0.29 mmol, 94%).^{1}H NMR (400 MHz, DMSO) δ 13.14 (s, 1H), 7.95 – 7.52 (m, 3H), 7.39 – 7.10 (m, 5H), 4.86 (d, *J* = 4.8, 1H), 3.06 (s, 2H), 2.92 (s, 2H), 1.55 (d, *J* = 4.5, 3H). ^{13}C NMR (101 MHz, DMSO) δ 171.13, 167.25, 167.11, 149.46, 140.79, 134.67, 131.68, 129.13, 128.43, 128.27, 125.99, 123.31, 123.19, 46.99, 36.99, 36.58, 14.88. LC-MS: *t*R: 7.97 min (linear gradient 10-90% in 13.5 min), m/z = 324.1 $[M+H]^+$,278.1 $[M-CO_2+H]^+$

Supplementary Information

Rit1 Crystallization

The data were integrated and scaled with the PROTEUM*plus* Crystallographic Software .

Table S1: Data collection and integration statistics for Rit1. The statistics in parentheses are for the highest resolution shell.

X-ray source	Cu-Kα rotating anode			
Wavelength (Å)	1.54146			
Detector	Bruker Nonius CCD area detector			
Temperature (°C)	-174°C (99K)			
Resolution range (Å)	40.52 – 2.3 (2.4-2.3)			
Crystal to film distance (mm)	60			
Exposure time (s)	10			
Oscillation per image (°)	0.5			
Space group	$P2_1$			
Mosaic spread (°)	~0.36			
Unit cell parameters (Å)	a (Å)	40.278	α (°)	90.0
	b (Å)	37.048	β (°)	95.90
	c (Å)	40.736	γ (°)	90.0
Total reflections	82115			
Unique reflections	5464			
Multiplicity	14.6 (3.75)			
Completeness (%)	98.0 (89.6)			
R_{sym}	0.0547 (0.163)			
$I/\sigma(I)$	36.45 (8.25)			

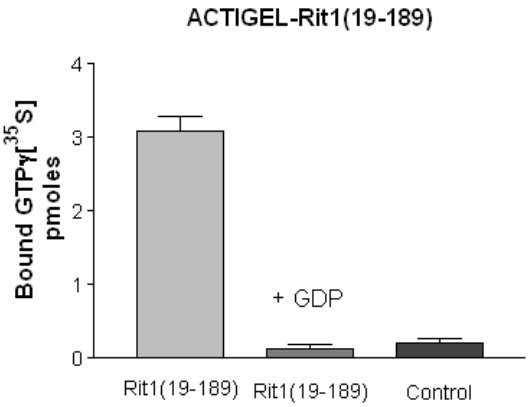

Figure S1. Nucleotide binding activity of the nucleotide-free form of immobilized Rit1 was determined using biochemical assay as described.

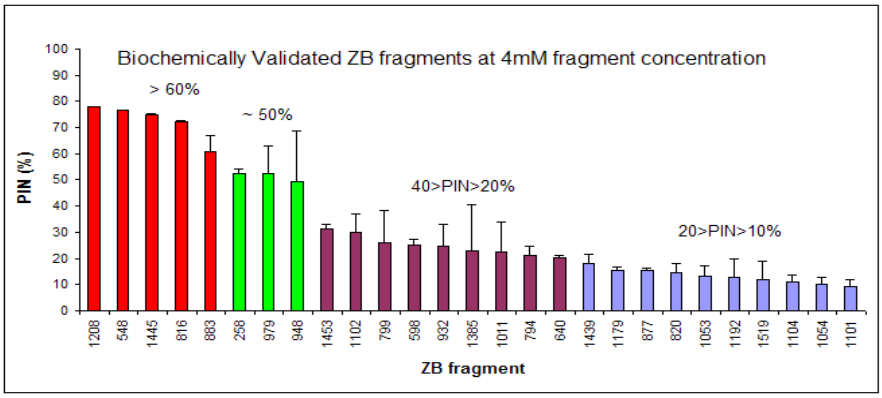

Figure S2. The ranking of primary fragment hits obtained from TINS NMR screening according to PIN % (percentage of inhibition) determined at high concentration in vitro biochemical assay.

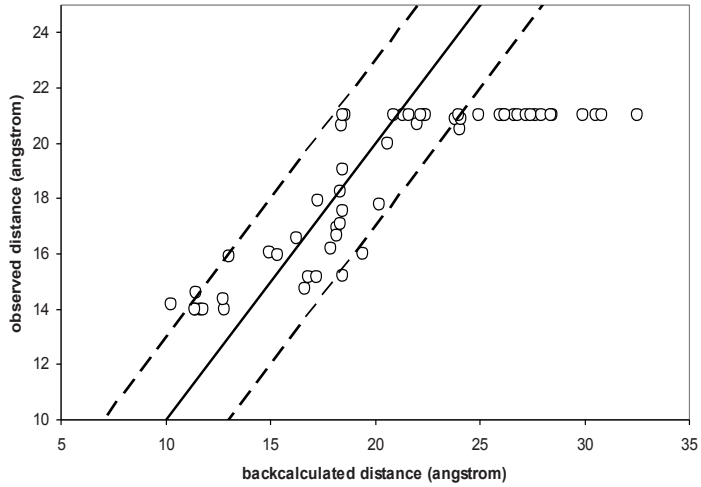

Figure S3. The experimentally observed nitroxide to amide proton distances (Å) are plotted against the back-calculated distances after optimizing the nitroxide position in XPLOR-NIH (see Methods). The solid line indicates the ideal correlation, dashed lines represent ± 3 Å error limits (Q =0.059). Amide protons of which the resonances were not affected by the nitroxide, were given a lower limit of 21 Å.

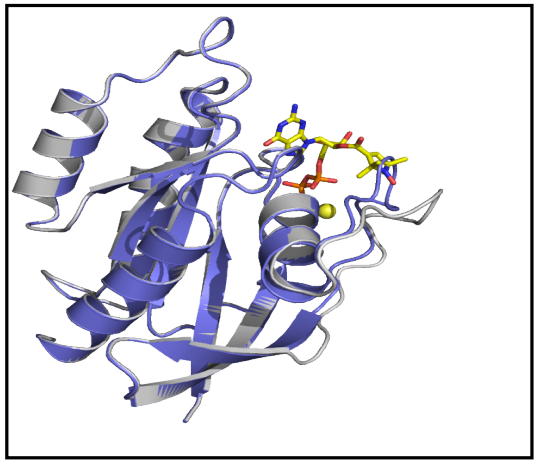

Figure S4. The loop consisting of residues 42-57 was optimized using PRE's observed from the nitroxide radical. In blue is the original crystal structure, yellow stick representing the position of the GDP-spin label, yellow sphere shows the magnesium ion and in the grey is the protein structure with the optimized loop position used for docking process.

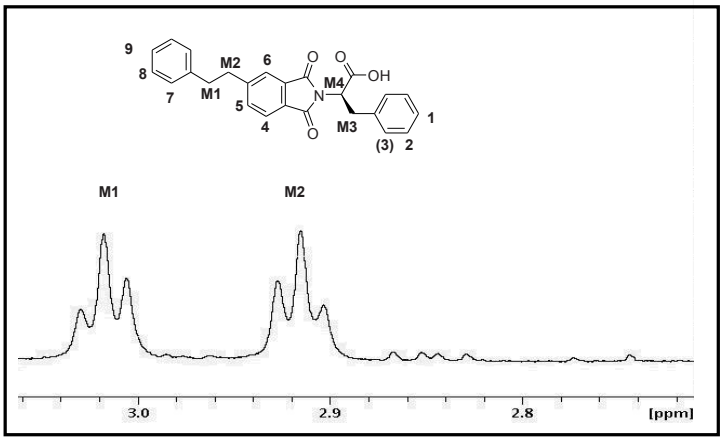

Figure S5. The two aliphatic resonances, M1 and M2 of **18c** are shown. Other resonances M3 and M4 could not be assigned due to overlap with the other buffer components.

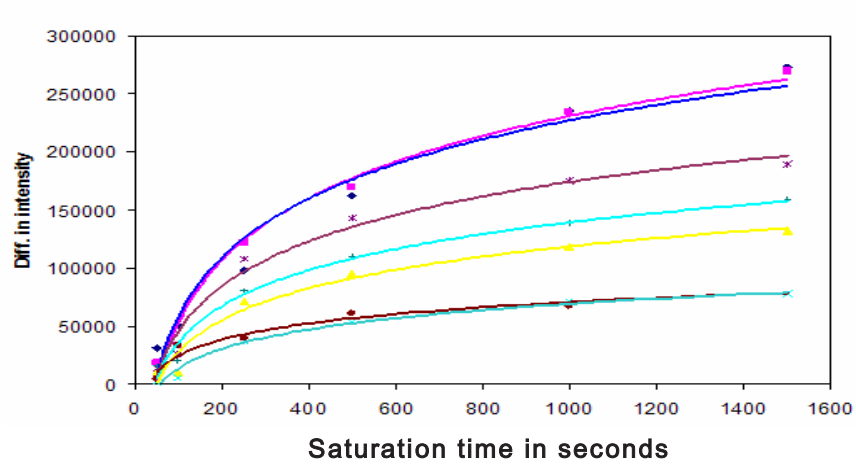

Figure S6. The saturation transfer experiments were performed as described in the experimental section. The plot of the intensity vs saturation time is depicted showing the saturation transfer rate for various protons of **18c**. The reduction in the intensity was caused by saturation transfer by irradiating at -0.5 ppm. The saturation time was varied from 50 ms to 2 sec.

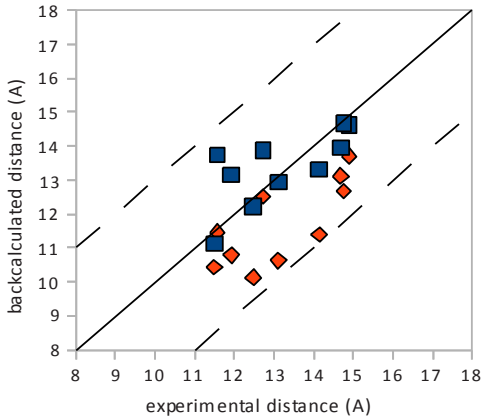

Figure S7. Comparison of back calculated and observed distances averaged over top 10 structures with error limits of ± 3A shown by dashed lines. Solid line represents the perfect correlation. The blue squares indicate the lowest docking solutions obtained by treating the intermolecular restraints as two separate sets. The red diamonds shows the distances obtained by simulation consisting of all inter-molecular PRE distance restraints in one set. As only two PRE restraints were available for the acidic moiety of **18c**, the force constant for PREs was increased from 3.0 to 90.0 to get a significant energy penalty whenever the PRE restraints were not fulfilled.

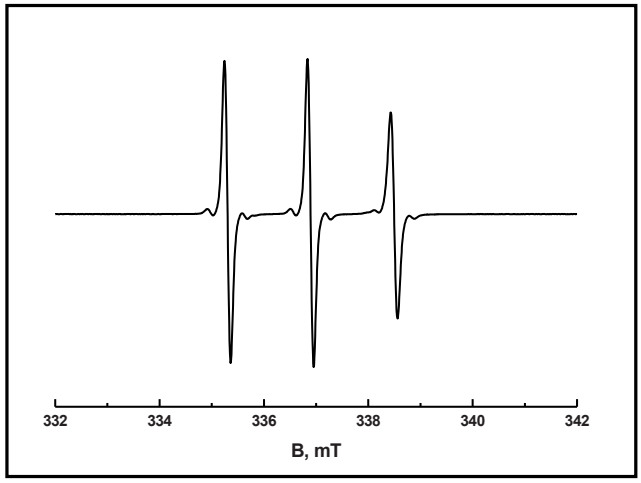

Figure S8. The X-band cw EPR measurements on GDP-spin label have been performed using an ELEXSYS E680 spectrometer (Bruker, Rheinstetten, Germany) equipped with a rectangular cavity. A modulation frequency of 100 kHz was used. Measurements were done at temperature of 20°C, using 6.31 mW of microwave power and modulation amplitude of 0.5 G.

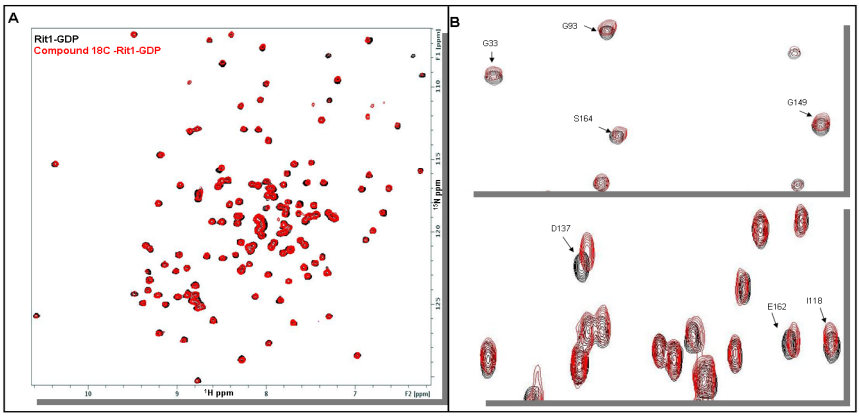

Figure S9. A] The overlay of the [^{1}H,^{15}N] HSQC spectra of Rit1-GDP (black) and in the presence of 1mM compound **18c** (red). B] The zoomed region of the overlaid [^{1}H, ^{15}N] HSQC NMR spectra shown in (A). The residues that show significant CSPs are labeled.

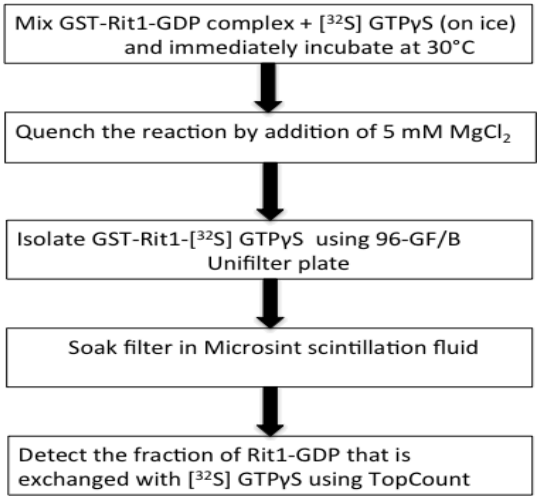

Figure S10. The diagrammatic representation of the nucleotide exchange assay used to determine IC_{50}'s of the inhibitory compounds.

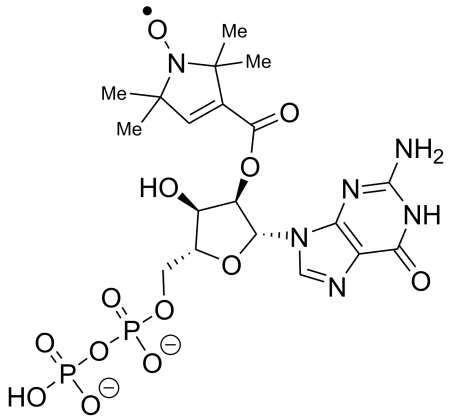

Figure S11. The depiction of the chemical structure of the GDP-spin label probe used in the paramagnetic NMR studies.

S12. Docking script used for the calculations in XPLOR-NIH:

```
!-----------------variables-----------------------------------
 eval ($a01 = 1)              ! cycle counter
 eval ($a02 = 20.0)           ! random distance max added
 eval ($a03 = 0.0)            ! prevents to throw two times
 eval ($a04 = 40.0)           ! structure writing threshold 27
 eval ($a05 = 10000)                ! nr cycles
 eval ($a06 = "cycle_1.pdb")        ! initial value saved structure
 eval ($a08 = 30.0)                 ! fbeta, frictinal constant
 eval ($a09 = 1.5)            ! velocity factor
 eval ($a10 = 180.0)                ! random rotation max +/-0.5*
 eval ($a11 = 1)              ! number of structures output per run
 eval ($a12 = $a11-1)               ! count saved structures
 eval ($a13 = $a04)           ! initial lowest energy filter
 eval ($a14 = 1)              ! initial value system energy
 eval ($a15 = 4000)           ! initial value system energy
 eval ($a16 = 4000)           ! initial value system energy
 eval ($a17 = 4000)           ! initial value system energy
 eval ($a18 = 1000)           ! initial value lowest energy from throw
 eval ($a19 = -1)             ! initial value count within throw
 eval ($a20 = 1)              ! count throws from minimum
 eval ($a21 = $cpu*1)         ! starting point random numbers
 eval ($a22 = 3.0)            ! force constant PRE
 eval ($a23 = 5.0)            ! force constant CSP
```

```
 eval ($a24 = 10.0)          ! force constant STD
 eval ($a25 = 4000)          ! initial value system energy
 eval ($a26 = 10)            ! Etot
 eval ($a27 = 10)            ! Evdw
 eval ($a28 = 10)            ! Enoe

!----------------ligand structure-------------------------------
set echo=off end
set mess=off end

 topology
   @/afs/gorlaeus.net/users/p/pkeizers/xplor/dipen/ligand/lig.top
 end

 param
   @/afs/gorlaeus.net/users/p/pkeizers/xplor/dipen/ligand/lig.par
 end

 segment
   name="lig"
   molecule number=1 name="lig" end
 end

 vector do (resi="500") (resn = "lig")
 vector do (segid="    ") (resn = "lig")
 coor @/afs/gorlaeus.net/users/p/pkeizers/xplor/dipen/ligand/lig.pdb
 vector do (segid="lig") (resi="500")

 flags exclude * include bonds angles impropers dihedrals end

 parameters
   learn initiate sele=(segid="lig") mode=nostatistics end
   learn accumulate end
   learn terminate end
 end

 parameters
   BOND   (segid "lig") (segid "lig") 400. TOKEN
   ANGLE  (segid "lig") (segid "lig") (segid "lig") 60. TOKEN
   IMPR  (segid "lig") (segid "lig") (segid "lig") (segid "lig") 50. TOKEN TOKEN
 end

 flags include vdw elec pvdw pele end
```

```
 hbuild
    ACCEptor=(all)
    phistep=10.0
 end

shake
  molecule (segid "lig")
end


!-----------------protein structure----------------------------
set echo=off end
set mess=off end

structure
  @/afs/gorlaeus.net/users/p/pkeizers/xplor/dipen/sl_struc/dip_sl.psf
end

param
  @/afs/gorlaeus.net/users/p/pkeizers/xplor/dipen/sl_struc/dip_sl.par
end

 if ($a01=1) then
  coor @/afs/gorlaeus.net/users/p/pkeizers/xplor/dipen/sl_struc/dip_sl.pdb
 end if

 while ($a01 LE $a05) loop calc
 eval ($a21=$cpu*1)
 set seed=$a21 end

   if ($a14 GE $a15) then
    if ($a14 GE $a16) then
     if ($a14 GE $a17) then
      if ($a14 GE $a25) then
       eval ($a20 = $a20 + 1) end
        if ($a01 > $a03) then
         eval ($a03 = $a01 + 1.0)
          coor @/afs/gorlaeus.net/users/p/pkeizers/xplor/dipen/sl_struc/dip_sl.pdb
          vector show element (X) (NAME CAW)
            eval ($UX=($result))
            vector show element (Y) (NAME CAW)
            eval ($UY=($result))
            vector show element (Z) (NAME CAW)
```

```
                eval ($UZ=($result))
                coor trans sele= (segid "lig") vect =(-$UX -$UY -$UZ) end
                !eval ($a20 = $a20 + 1) end
                vector do (fbeta = $a08) (segid="lig")
                vector do (vx = $a09) (segid="lig")
                vector do (vy = $a09) (segid="lig")
                vector do (vz = $a09) (segid="lig")
                eval ($dist1=(40 + (RANDOM()*$a02)))
                eval ($ang1=(0.5 - RANDOM())*$a10)
                eval ($v1=(0.5 - RANDOM())*20)
                eval ($v2=(0.5 - RANDOM())*20)
                eval ($v3=(0.5 - RANDOM())*20)
                coor trans SELE=(segid="lig") VECT= ($v1 $v2 $v3) DIST = $dist1
end
                coor rota SELE=(segid="lig") cent= (0 0 0) axis ($v3 $v1 $v2) $ang1
end
              end if
             end if
            end if
           end if
          end if

        parameter
          nbonds
            inhi = 0.75
            ctofnb = 7.5 !5.0 default settings no sign. effect Etot
            ctonnb = 6.5 !4.0 default settings no sign. effect Etot
            repe1 = 0.8 !0.9 has severe effects Etot
            rexp = 2
            irex = 2
            rcon = 0.4 !0.1 may do the trick, adapt threshold too 0.3
          end
        end

        !-----------------DEFINE RESTRAINTS-----------------------------------

        !----------------- PRE restraints---------------------------------------
        if ($a01=1) then
          noe reset end
            NOE
              nrestraints=100000
            end
```

```
NOE
  class CL1
end

NOE
  assign (segid="lig" and name 1HAA) (segid= "dip" and name OBI) 13.11
3.0 3.0
  assign (segid="lig" and name 1HAD) (segid= "dip" and name OBI) 12.48
3.0 3.0
  assign (segid="lig" and name 1HAB) (segid= "dip" and name OBI) 11.92
3.0 3.0
  assign (segid="lig" and name 1HBA) (segid= "dip" and name OBI) 14.14
3.0 3.0
  assign (segid="lig" and name 1HBD) (segid= "dip" and name OBI) 14.76
3.0 3.0
  assign (segid="lig" and name 1HAZ) (segid= "dip" and name OBI) 14.68
3.0 3.0
 assign (segid="lig" and name 1HZ)  (segid= "dip" and name OBI) 14.89 3.0
3.0
 assign (segid="lig" and name 1HE2) (segid= "dip" and name OBI) 12.73 3.0
3.0
  assign (segid="lig" and name 1HAW) (segid= "dip" and name OBI) 11.56
3.0 3.0
  assign (segid="lig" and name 1HAX) (segid= "dip" and name OBI) 11.50
3.0 3.0
end

NOE
  averaging CL1 R-6
  potential CL1 square
  sqconstant CL1 0.005
  sqoffset CL1 0.0
  scale CL1 $a22
  sqexponent CL1 2
end

!--------------------CSP restraints----------------------------
NOE
   class CL2
end

NOE
   assign (atom "lig" * *H*) (resid 137 and name HN)  6.0 3.0 3.0
```

```
      assign (atom "lig" * *H*) (resid 167 and name HN)  6.0 3.0 3.0
      assign (atom "lig" * *H*) (resid 170 and name HN)  6.0 3.0 3.0
      assign (atom "lig" * *H*) (resid 162 and name HN)  6.0 3.0 3.0
      assign (atom "lig" * *H*) (resid 136 and name HN)  6.0 3.0 3.0
      assign (atom "lig" * *H*) (resid 173 and name HN)  6.0 3.0 3.0
      assign (atom "lig" * *H*) (resid 169 and name HN)  6.0 3.0 3.0
      assign (atom "lig" * *H*) (resid 168 and name HN)  6.0 3.0 3.0
      assign (atom "lig" * *H*) (resid 164 and name HN)  6.0 3.0 3.0
      assign (atom "lig" * *H*) (resid 163 and name HN)  6.0 3.0 3.0
      assign (atom "lig" * *H*) (resid 139 and name HN)  6.0 3.0 3.0
      assign (atom "lig" * *H*) (resid 116 and name HN)  6.0 3.0 3.0
      assign (atom "lig" * *H*) (resid 113 and name HN)  6.0 3.0 3.0
    end

    NOE
      averaging CL2 R-6
      potential CL2 square
      sqconstant CL2 0.005
      sqoffset CL2 0.0
      scale CL2 $a23
      sqexponent CL2 2
    end

!--------------------STD restraints----------------------------
    NOE
      class CL3
    end

    NOE
      assign (atom "lig" * *H*) (atom "dip" * C*)  5.0 3.0 4.0
    end

    NOE
      averaging CL3 R-6
      potential CL3 square
      sqconstant CL3 0.005
      sqoffset CL3 0.0
      scale CL3 $a24
      sqexponent CL3 2
    end
  end if

!--------------------dock ligand--------------------------------
```

```
 constraints
  interactions (segid="dip" or segid="lig")
  (segid="lig") end
 constraints
  FIX (not (segid="lig")) end

 flag exclude * include bond angle dihe impro noe vdw end

 minimize powell
  nstep = 200
  nprint = 200
  drop = 10
 end

 constraints
  interactions ((segid="dip" and (name CA or name C or name O or name N
or name
  HN or name CB or name CG or resi 186)) or segid="lig")
  (segid="lig") end
 constraints
  FIX (not (segid="lig")) end

 flag exclude * include noe bond angle impro dihe vdw end

 vector do ( fbeta = 6.657235 ) ( segid="lig" )
  dynamics langevin
  timestep = 0.001
  nstep = 2500
  ilbfrq = 2500
  nprint = 2500
  tbath = 300.
  iasvel = maxwell
  rbuf = 0.0
  origin = ( 0. 0. 0. )
 end

!------------optimize sidechains-------------------------------
 constraints
  interactions (segid="dip" or segid="lig")
  (segid="lig" or segid="dip") end
 constraints
  FIX (segid="dip" and (name CA or name C or name O or name N or name
```

```
  HN or name MG or name CM or resi 186)) end
 flag exclude * include noe bond angle impro dihe vdw end

 vector do ( fbeta = 6.657235 ) ( segid="lig" )
  dynamics langevin
   timestep = 0.001
   nstep = 1500
   ilbfrq = 1500
   nprint = 1500
   tbath = 300.
   iasvel = maxwell
   rbuf = 0.0
   origin = ( 0. 0. 0. )
  end

!------------calculate energies and write structures-------------
 flag exclude * include noe vdw end
 energy end

 set disp=ener.dat end
  if ($a01=1) then
        display file: ener.dat          $DATE $TIME
        display
        display cycle Etot    Evwd  Enoe  structure       number         time
  end if
  eval ($a25 = $a17)
  eval ($a17 = $a16)
  eval ($a16 = $a15)
  eval ($a15 = $a14)
  eval ($a14 = $ENER)
  eval ($a07 = ($a20 - $a19))
   if ($a07 = 1) then
    coor swap end
    write coord output = $a06 end
    display $a01      $a26   $a27   $a28   $a06   $a11   $TIME
    set disp=OUTPUT end

    eval ($a12 = $a11)
    eval ($a11 = $a11 +1)
    coor swap end
   end if
    if ($a14 LE $a04) then
     if ($a07 LE 0) then
```

```
      if ($a14 LE $a18) then
       coor copy end
       eval ($a26 = $ener)
         eval ($a27 = $vdw)
         eval ($a28 = $noe)
         eval ($a18 = $a14)
       eval ($a12 = $a12 + 1)
        if ($a14 LE $a13) then
         eval ($a13 = $a14)
        end if
       eval ($a19 = $a20)
      end if
     end if
      if ($a07 > 0) then
         coor copy end
       eval ($a26 = $ener)
         eval ($a27 = $vdw)
         eval ($a28 = $noe)
         eval ($a06 = "cycle_"+encode($a11)+".pdb")
        if ($a14 LE $a13) then
         eval ($a13 = $a14)
        end if
       eval ($a18 = $a14)
       eval ($a12 = 0)
         eval ($a19 = $a20)
      end if
    end if
  eval ($a01 = $a01 + 1)
 end loop calc

!---------------------------------------------------------------
!----------------------FINISH-----------------------------------
!---------------------------------------------------------------
stop
```

Contributions

Target identification, validation and production of protein for crystallography, nucleotide exchange assays and NMR screening were performed by Masakazu Kobayashi (Galapagos NV). NMR screening was performed at ZoBio BV. Johan Hollander (ZoBio BV) helped to set-up the NMR screen. Eiso AB and Caroline Loch (ZoBio BV) performed the computational analysis to generate fragments hits. Francis Figaroa (ZoBio BV) assisted with the compound preparations for TINS NMR screen. Anna A. Rzepiela (Pyxis discovery) performed the computational studies for analogs. Crystallography studies on the target and target-ligand complexes were performed by F. Hoedemaker and Linda Manning (KeyDP BV). Synthesis of compounds at various stages was done by Adriaan W.Tuin (Leiden University). Peter H.J. Keizers (Leiden University) performed the computational docking for paramagnetic restraints.

REFERENCES

(1) Quan, L., Thiele, G., Tian, J. and Wang, D. The development of novel therapies for Rheumatoid Arthritis. *Expert Opin Ther Pat*, **2008**, 18(7), 723–738.

(2) Methods for Identification, and Compounds useful; for the treatment of degenerative andnflammatory diseases, Ser. No. 11/52,366, filed Jun.14, **2005** Galapagos B.V. US patent 7,919,259 B2.

(3) Colicelli, J. Human RAS Superfamily Proteins and Related GTPases *Sci. STKE*, **2004**, 250, 13.

(4) Wennerberg, K., Rossman. L.K., Channing, J D. The Ras superfamily at a glance *J. Cell. Sci.* **2005,** 118, 843-846**.**

(5) Gorfe, A. A. Mechanisms of allostery and membrane attachment in Ras GTPases: implications for anti-cancer drug discovery**.** *Curr Med Chem*, **2010**, 171-9**.**

(6) Hall, B., Bar-Sagi, D., Nassar, N. The structural basis for the transition from Ras-GTP to Ras-GDPPNAS, *Proc Natl Acad Sci*. **2002**, 99(19), 12138-12142.

(7) Kinbara, K., Goldfinger,LE., Hansen, M., Chou, F and Ginsberg, M. Ras GTPases: integrins' friends or foes *Nature Rev. Mol Cell Biol.* **2003**, 4, 767-778.

(8) Walker, K., Olson, M. Targeting Ras and Rho GTPases as opportunities for cancer therapeutics. Curr. Opinion in Gen. & Development **2005**, 15(1), 62-68.(9) Bell, I.M., Gallicchio, S.N., Abrams, M., Beese, L., Beshore, D., Bhimnathwala, H., Bogusky, M., Buser, C., Culberson, J., Davide, J. 3-Aminopyrrolidinone farnesyl transferase inhibitors: Design of macrocyclic compounds with improved pharmacokinetics and excellent cell potency *J Med Chem*, **2002**,45, 2388–2409.

(10) Hunt, J., Ding, C., Batorsky, R., Bednarz, M., Bhide, R., Cho, Y., Chong, S., Gullo-Brown, J., Guo P. Discovery of (R)-7-cyano-2,3,4, 5-tetrahydro-1-(1H-imidazol-4-ylmethyl)-3- (phenylmethyl)-4-(2-thienylsulfonyl)-1H–1,4-benzodiazepine (BMS-214662), a farnesyl transferase inhibitor with potent preclinical antitumor activity. *J Med Chem*, **2000**, 43, 3587–3595.

(11) Zhang, FL and Casey, PJ., Protein prenylation: molecular mechanisms and functional consequences. *Annu Rev Biochem*, **1996**, 65, 241–269.

(12) Konstantinopoulos, P., Karamouzis, M., Papavassiliou, A. Post-translational modifications and regulation of the RAS superfamily of GTPases as anticancer targets. *Nat Rev Drug Disc,* **2007**, 6, 541-555.

(13) Hynds, D., Spencer, ML., Andres, D., Snow, D. Rit promotes MEK-independent neurite branching in human neuroblastoma cells. *J Cell Sci*, **2004**, 116 (10), 1925–35.

(14) Shao, H., and Andres, D. A novel RalGEF-like protein, RGL3, as a candidate effector for rit and Ras. *J Biol Chem*, **2000**, 275 , 26914–26924.

(15) Andres, D., Rudolph, J., Sengoku, T., and Shi, GX. Analysis of Rit Signaling and Biological Activity. *Meth Enzymol*, **2006**,407, 499-512.

(16) Rusyn, E., Reynolds, E., Shao, H., Grana, T., Chan, T., Andres, D., and Cox, A. Rit, a non-lipid-modified Ras-related protein, transforms NIH3T3 cells without activating the ERK, JNK, p38 MAPK or PI3K/Akt pathways. *Oncogene*, **2000**,19, 4685–4694.

(17) Hajduk,P.J., Greer, J. A decade of fragment-based drug design: Strategic advances and lesson learned. *Nat Rev Drug Disc*, **2007**, 6, 211-219.

(18) Scheffzek, K., Ahmadian, M., Kabsch, W., Wiesmüller, L., Lautwein, A., Schmitz, F and Wittinghofer, A. The Ras-RasGAP Complex: Structural Basis for GTPase Activation and Its Loss in Oncogenic Ras. *Mut Sci*, **1997**, 277, 333-339.

(19) Karassek, S., Berghaus, C., Schwarten, M., Emans, C., Ohse, N., Kock, G., Jockers, K., Neumann, S., Gottfried, S., Herrmann, C., Heumann, R., and Stoll, R. Ras homolog enriched in brain (Rheb) enhances apoptotic signaling. *J Biol Chem*, **2010**, 285 (44) 33979-33991.

(20) Vanwetswinkel, S., Heetebrij, RJ., van Duynhoven, J., Hollander JG., Filippov DV., Hajduk PJ., Siegal, G.TINS: Target Immobilized NMR Screening – An efficient and sensitive new method for ligand discovery. *Chem Biol*, **2005**, 12, 207-216.

(21) Marquardsen, T., Hofmann, M., Hollander, J., Loch, C., Kiihne, S., Engelke, F., and Siegal, G. Development of a dual cell, flow-injection sample holder and NMR probe for comparative ligand-binding studies. *J Mag Reson*, **2006**, 182, 55-65.

(22) John, J., Sohmen, R., Feuerstein, J., Linke, R., Wittinghofer, A., Goody, R. Kinetics of interaction of nucleotides with nucleotide-free H-ras p21.*Biochem*, **1990**, 29(25), 6058–6065.

(23) Siegal, G., AB, Eiso and Schultz, J. Integration of Fragment Screening and Library Design, *Drug Disc Today*, **2007**, 12,1032-1039.

(24) Taveras, AG., Remiszewski, SW., Doll, RJ., Cesarz, D., Huang, EC., Kirschmeier, P., Pramanik, BN., Snow, ME., Wang, YS., del Rosario, JD., Vibulbhan, B., Bauer, BB., Brown, JE., Carr, D., Catino, J., Evans, CA., Girijavallabhan, V., Heimark, L., James, L., Liberles, S., Nash, C., Perkins, L., Senior, MM., Tsarbopoulos, A., Webber, SE. *Bioorg Med* Chem,**1997**, 5(1), 125-133.

(25) Ganguly, AK., Wang, YS., Pramanik, BN., Doll, RJ., Snow, ME., Taveras, AG., Remiszewski, S., Cesarz, D., del Rosario, J., Vibulbhan, B., Brown, JE., Kirschmeier, P., Huang, EC., Heimark, L., Tsarbopoulos, A., Girijavallabhan, VM., Aust, RM., Brown, EL., DeLisle, DM., Fuhrman, SA., Hendrickson, TF., Kissinger, CR., Love, RA., Sisson, WA., Webber, SE. Interaction of a novel GDP exchange inhibitor with the Ras protein. *Biochem*, **1998**, 37(45):15631-7.

(26) Peri, F., Airoldi, C., Colombo, S., Mari, S., Jiménez-Barbero, J., Martegani, E., and Nicotra F. Sugar-derived Ras inhibitors: group epitope mapping by NMR spectroscopy and biological evaluation. *Euro J Org Chem*, **2006**, 3707-3720.

(27) Hajduk, PJ., Huth, JR., and Fesik, SW. Druggability indices for protein targets derived from NMR-based screening data. *J Med Chem*, **2005**,48, 2518-2525

(28) McCoy, MA., Wyss, DF. Spatial localization of ligand binding sites from electron current density surfaces calculated from NMR chemical shift perturbations. *J Am Chem Soc*, **2002** 124, 11758–11763.

(29) The PyMOL Molecular Graphics System, Version 1.2r3pre, Schrödinger, LLC

(30) Olsen, J., De Godoy, L., Li, G., Macek, B., Mortensen, P., Pesch, R., Makarov, A.,
Lange, O., Horning, S., Mann, M. Parts per million mass accuracy on an Orbitrap mass spectrometer via lock mass injection into a C-trap. *Mol Cell Proteo*, **2005**, 4, 2010–2021.

(31) Zav'yalov, S., Dorofeeva, O., Rumyantseva, E., Kulikova, L., Ezhova, G. Synthesis of N-Phthaloyl Derivatives of Amino Acids, *Phar Chem Jour,* **2002**, 36, 440 – 442

(32) Nakamura, T., Noguchi, T., Kobayashi, H., Miyachi, H., and Hashimoto, Y. Mono- and dihydroxylated metabolites of thalidomide: synthesis and TNF-alpha production-inhibitory activity. *Pharm. Bull*, **2006**. 54, 1709—1714

(33) Bodenhausen, G., and Ruben, D. Natural abundance nitrogen-15 NMR by enhanced heteronuclear spectroscopy. *Chem Phys Lett*, **1980**, 69 (1), 185-189.

(34) Sklenar, V., Piotto, M., Leppik, R., and Saudektim, V. Gradient-Tailored Water Suppression for ^{1}H - ^{15}N HSQC Experiments Optimized to Retain Full Sensitivity. *J Magn Reson*, **1993**, (A) 102, 241 -245.

(35) Bashir, Q., Volkov, A., Ullmann, GM., and Ubbink, M. Visualization of the encounter ensemble of the transient electron transfer complex of cytochrome *c* and cytochrome *c* peroxidase *J Am Chem Soc*, **2010,** 132**,** 241-247.

(36) Schwieters, C. D., Kuszewski, J. J., Tjandra, N., and Clore, G. M. The Xplor-NIH NMR molecular structure determination package. *J Magn Reson*, **2003**, 160, 65– 73.

(37) Mayer, M., and Meyer, B. Group Epitope Mapping (GEM) by STD NMR to identify segments of a ligand in direct contact with a protein receptor, *J Am Chem Soc*, **2001**, 123, 6108- 6117.

(38) Mayer., M and Meyer, B. A fast and sensitive method to characterize ligand binding by saturation transfer difference NMR spectra, *Angew Chem*, **1999**, 111, 1902-1906.

(39) Mayer., M and Meyer, B. Characterization of Ligand Binding by Saturation Transfer Difference NMR Spectroscopy. *Angew Chem Int Ed*, **1999**, 38, 1784-1788.

(40) Wüthrich K. NMR of Proteins and Nucleic Acids. New York: Wiley and Sons, **1986**.

(41) Muraoka, S., Shima, F., Araki, M., Inoue, T., Yoshimoto, A., Ijiri, Y., Seki, N., Tamura, A., Kumasaka, T., Yamamoto, M, Kataoka, T. Crystal structures of the state 1 conformations of the GTP-bound H-Ras protein and its oncogenic G12V and Q61L mutants. *FEBS Lett*, **2012**, 586(12), 1715-8.

(42) Maurer, T., Garrenton, LS., Oh, A., Pitts, K., Anderson, DJ., Skelton, NJ., Fauber, BP., Pan, B., Malek, S., Stokoe, D., Ludlam, MJ., Bowman, KK., Wu, J., Giannetti, AM., Starovasnik, MA., Mellman, I., Jackson, PK., Rudolph, J., Wang, W., Fang, G. Small-molecule ligands bind to a distinct pocket in Ras and inhibit SOS-mediated nucleotide exchange activity. *Proc Natl Acad Sci*, **2012,**109(14), 5299-304.

(43) Shao, H., Kadono-Okuda, K., Finlin, B. S. and Andres, D. A.. Biochemical characterization of the Ras-related GTPases Rit and Rin. *Arch Biochem Biophys*, **1999,** 371*,* 207 -219.

(44) The CCP4 Suite: Programs for Protein Crystallography. Collaborative Computational Project, Number 4. *Acta Cryst*, **1994**, D50, 760-763.

(45) Emsley, P., Cowtan, K., Coot: model-building tools for molecular graphics. *Acta Crystallogr*, **2004**, D60, 2126-2132.

(46) Kobayashi, M., Retra, K., Figaroa, F., Hollander, JG., Ab, E. Heetebrij, RJ., Irth, H., Siegal, G. Target immobilization as a strategy for NMR based fragment screening. Comparison if TINS, STD and SPR for fragment hit identification. *J Biomol Screen*, **2010**, 15(8), 978-989.

(47) Murali, N., Miller, WM., John, BK., Avizonis, DA. Smallcombe SH spectral unraveling by space-selective Hadamard spectroscopy*. J Magn Reson,* **2006***,*179*,*182-189*.*

(48) NMRPipe: a multidimensional spectral processing system based on UNIX pipes. Delaglio, F., Grzesiek, S., Vuister, GW., Zhu, G., Pfeifer, J., and Bax, A. *J Biomol NMR*, **1995**, 6(3), 277-93.

(49) Goddard, TD., and Kneller, DG. SPARKY 3, University of California, San Francisco.

(50) Jung, YS., and Zweckstetter, M. Mars-robust automatic backbone assignment of proteins. *J Biomol NMR*, **2004**, 30(1), 11—23.

(51) Lin, B., Covalle, KL., Maddock, JR.The Caulobacter crescentus CgtA protein displays unusual guanine nucleotide binding and exchange properties, *J Bacteriol*, **1999**,181(18), 5825–5832.

(52) Lenzen, C., Cool, RH., Wittinghofer, A. Analysis of intrinsic and CDC25-stimulated guanine nucleotide exchange of p21ras-nucleotide complexes by fluorescence measurements. *Methods Enzymol*. **1995**;255:95-109

(53) Streckenbach, B., Schwarz, D., and Kurt, R.H. Repke Analysis of phosphoryl transfer mechanism and catalytic centre geometries of transport ATPase by means of spin-labelled ATP *Biochimic et Biophysic Acta Biomem*, **1980**, 601, 34-46.

(54) Ferguson, K., Higashijima, T., Smigel, MD., and Gilman, A. The influence of bound GDP on the kinetics of Guanine Nucleotide binding to G proteins. *J Biol Chem*, **1986**, 261(16), 7393-7399.

(55) Keizers, P., Saragliadis, A., Hiruma, Y., Overhand, M., and Ubbink, M. Design, synthesis, and evaluation of a lanthanide chelating protein probe: CLaNP-5 yields predictable paramagnetic effects independent of environment, *J Am Chem Soc*, **2008**,130 (44),14802–14812.

(56) Schüttelkopf, AW., and van Aalten, D. PRODRG - a tool for high-throughput crystallography of protein-ligand complexes, *Acta Crystallogr,* **2004** D60, 1355–1363.